Universidade de Aveiro Departamento de Física
2018

Rui Filipe Oliveira Ruela

Influência das Alterações Climáticas na Temperatura da Superfície do Mar a Nível Mundial

Worldwide Evolution of Sea Surface Temperature Under Climate Change

Universidade de Aveiro Departamento de Física
2018

Rui Filipe Oliveira Ruela

Influência das Alterações Climáticas na Temperatura da Superfície do Mar a Nível Mundial

Worldwide Evolution of Sea Surface Temperature Under Climate Change

Dissertação apresentada à Universidade de Aveiro para cumprimento dos requisitos necessários à obtenção do grau de Mestre em Ciências do Mar e da Atmosfera, realizada sob a orientação científica do Doutor João Miguel Sequeira Silva Dias, Professor Associado c/ Agregação do Departamento de Física da Universidade de Aveiro, e da Doutora Magda Catarina Ferreira de Sousa, Estagiária de Pós-Doutoramento do CESAM da Universidade de Aveiro.

A toda a minha família e amigos que me acompanharam ao longo de todo o meu percurso académico.

o júri

Presidente	Prof. Doutor José Manuel Henriques Castanheira Professor Auxiliar do Departamento de Física da Universidade de Aveiro
Arguente	Prof. Doutora María Teresa de Castro Rodríguez Professora Titular do Departamento de Física Aplicada da Faculdade de Ciências de Ourense, Universidade de Vigo
Orientador	Prof. Doutor João Miguel Sequeira Silva Dias Professor Associado c/ Agregação do Departamento de Física da Universidade de Aveiro

agradecimentos /
acknowledgements

Despite all my dedication to this work, I would not be able to conclude it without the help of several people.

Firstly, I would like to begin by thanking my supervisor, Prof. Dr. João Miguel Dias, for his patience and guidance throughout this work.

I am also grateful to my co-supervisor, Dr. Magda Sousa, for her technical support, suggestions, and patience during this research. Her programming skills were always an inspiration to continue my research.

I would like also to thank all my colleagues of NMEC (Estuarine and Coastal Modelling Division) for sharing their knowledge with me and for welcoming me in the best way.

I would thank the Prof. Ines Alvarez for suggested and following my work and receiving me in the best way in EphysLab.

To my family and friends, for their support, comprehension, and encouragement at the most difficult moments. I am speccially grateful to Joana Mendes and Beatriz Gomes for their support along this dissertation.

Palavras Chave Variabilidade da TSM, CMIP5, aquecimento global, alterações climáticas

Resumo

As alterações climáticas referem-se a alterações substanciais nas medidas do clima que duram por um período prolongado, sendo a temperatura da superfície do mar (TSM) uma forma importante de detetar e investigar as suas causas e efeitos. Assim, o principal objetivo desta dissertação é compreender os impactos das alterações climáticas na TSM a nível mundial através da análise de dados de TSM dos modelos globais (GCM) do projeto CMIP5. A metodologia adotada seguiu duas etapas fundamentais: 1) divisão mundial de dados TSM em regiões através do método K-means cluster e validação das previsões dos modelos globais através da sua comparação com dados da plataforma de reanálises Era Interim; 2) calcular as diferenças entre dados climáticos futuros (2070-2100 e 2020-2050) e históricos (1975-2005) para os cenários climáticos RCP4.5 e RCP 8.5 e calcular as tendências entre 1975 e 2100 para ambos os cenários de RCP. Os dados de TSM foram divididos em oito regiões. A maioria dos modelos globais apresentam boa reprodutibilidade da TSM. As regiões do Hemisfério Norte apresentam maior amplitude térmica quando comparadas com as regiões equivalentes do Hemisfério Sul. As diferenças entre o futuro longínquo e o regime histórico são maiores do que as diferenças entre o futuro próximo e o regime histórico. Para o futuro a longo prazo, a TSM mundial apresenta aumentos médios de 2.46 ºC e 1.35 ºC para os cenários RCP 8.5 e RCP 4.5, respectivamente. Para o futuro próximo, a TSM tem incrementos médios de 0.86 ºC e 0.73 ºC para os cenários RCP 8.5 e RCP 4.5, respectivamente. As regiões polares apresentam maior variabilidade percentual, sendo possível concluir que estas apresentam maiores alterações, refletindo um superaquecimento nessas regiões. Para o cenário RCP 8.5, a TSM apresenta tendências de 4.34 ºC/dec (máximo) e 1.64 ºC/dec (mínimo) para as regiões sub-tropical norte (STRN) e polar sul (PRS), respectivamente. Relativamente ao cenário RCP 4.5, a TSM apresenta tendências de 2.64 ºC/dec (máximo) e 0.94 ºC/dec (mínimo) para STRN e PRS, respectivamente. Este trabalho permitiu concluir que não é possível selecionar apenas um modelo global, pois cada um tem as suas vantagens. O Hemisfério Norte apresenta tendências de súbida da TSM mais acentuadas. No geral, os resultados demonstram que a TSM aumentará em todo o globo, embora este acréscimo dependa de cada região.

Keywords SST variability, CMIP5, global warming, climate changes

Abstract

Climate changes refer to any substantial changes in measures of climate lasting for an extended period. One the important ways to track and investigate the causes and effects of climate change is through the use of indicators, like sea surface temperature (SST). Thus, the main aim of this dissertation is to understand the impacts of climate changes in future SST variability with analysis of SST data from global climate models (GCMs) of CMIP5 project. The methodology adopted comprised two fundamental steps: 1) worldwide SST data division in regions with K-means cluster and validation of CMIP5 models with a comparative analysis between SST data of CGMs of CMIP5 and SST data of Era Interim reanalysis; 2) calculate differences between future (2070-2100 and 2020-2050) and historical (1975-2005) SST data for RCP4.5 and RCP 8.5 climatic scenarios, and compute trends between 1975 and 2100 for both RCP scenarios.

SST data of CGMs of CMIP5 are divided into eight regions. Most of GCMs of CMIP5 have a good SST reproducibility. North Hemisphere regions present a higher thermal amplitude when compared with equivalent regions of South Hemisphere. The differences between long-term future and historical regime are larger than differences between near-term future and historical regime. For long-term future, worldwide SST has mean increments of 2.46 ºC and 1.35 ºC for RCP 8.5 and RCP 4.5 scenarios, respectively. For near-term future, SST has mean increments of 0.86 ºC and 0.73 ºC for RCP 8.5 and RCP 4.5 scenarios, respectively. Polar Regions present higher percentual variability, being possible to conclude that Polar Regions will have larger changes, reflecting an overheating on these regions. For RCP 8.5 scenario, SST trends are 4.34 ºC/dec (maximum) and 1.64 ºC/dec (minimum) for north sub-tropical region (STRN) and south polar region (PRS), respectively. Regarding RCP 4.5 scenario, SST trends are 2.64 ºC/dec (maximum) and 0.94 ºC/dec (minimum) for STRN and PRS, respectively. From this work it can be concluded that is not possible to select only one global model, since each has its advantages. North Hemisphere will present higher SST trends. Overall, this thesis analysis has revealed that SST will increase worldwide, however, this depends on the different globe locations.

Contents

List of Figures

List of Tables

Nomenclature

η	Normalized Correlation
CMIP5	Coupled Model Intercomparison Project Phase 5
Co	Correlation
ERN	North Equatorial Region
ERS	South Equatorial Region
k	Number of clusters
KS-test	Kolmogorov-Smirnov test
Me	Metrics
MW-test	Mann-Whitney test
NAO	North Atlantic Oscillation
PRN	North Polar Region
PRS	South Polar Region
RCP	Representative Concentration Pathways
RMSD	Root Mean Square Deviation
SAT	Surface Air Temperature
SD	Standard Deviation
SST	Sea Surface Temperature
STRN	North Sub-Tropical Region
STRS	South Sub-Tropical Region
TRN	North Tropical Region
TRS	South Tropical Region

1 Introduction

1.1 Motivation and aims

The Earth's climate is changing. Temperatures are rising, snow and rainfall patterns are shifting, and more extreme climate events are occuring, like heavy rainstorms and heat waves. Scientists found that many of these observed changes can be linked to the levels of carbon dioxide and other greenhouse gases in our atmosphere, which have increased because of human activities (Environmental Protection Agency, 2016).

Climate change is a change in the statistical distribution of weather patterns when that change lasts for an extended period of time (i.e., decades to millions of years). Climate change may refer to a change in average weather conditions, or in the time variation of weather within the context of longer-term average conditions, defined by the World Meteorological Organization as a 30 years or longer term. Natural factors have caused the climate to change during previous periods of the Earth's history, but human activities are considered the actual main cause and the accelerator of the changes that are being observed now.

Past studies indicated that it is extremely likely that there has been a substantial anthropogenic contribution to global and continental surface air temperature (SAT) increases since the middle of the 20^{th} century (Hegerl *et al.*, 2007; Bindoff *et al.*, 2014).

Since the industrial revolution began in the 1700s, humans have added a significant amount of greenhouse gases into the atmosphere, largely by combustion of fossil fuels to generate electricity, heat and cool buildings, and power vehicles – as well as by dissipating forests. The major greenhouse gases that humans have added to the atmosphere are carbon dioxide, methane, nitrous oxide, and fluorinated gases. When these gases are emitted into the atmosphere, many remain there for long time periods, ranging from a decade to thousands of years. Previous emissions affect the earth atmosphere in the present days. Current and future emissions will continue to increase the levels of these gases in the atmosphere for the foreseeable future (Environmental Protection Agency, 2016).

Greenhouse gases got their name because they trap heat (energy) like a greenhouse in the lower part of the atmosphere. As more of these gases are added to the atmosphere, more heat is trapped. This extra heat leads to higher air temperatures near the Earth's surface, alters weather patterns, and raises the temperature of the oceans.

Global warming is a term often used interchangeably with the term "climate change", but they do not represent the same process. Global warming refers to an average increase in the temperature of the atmosphere near the Earth's surface. Global warming is just one aspect of global climate change, however a very important one.

The changes observed in the world are affecting people and the environment in a crucial way. For example, sea levels are rising, glaciers are melting, and plant and animal life cycles are changing. These types of changes can bring fundamental disruptions in ecosystems, affecting plant and animal populations, communities and biodiversity. Such changes can also affect people's health and quality of life, including the places where people can live, what kinds of crops are most viable, what kinds of businesses can thrive in certain areas, and the condition of buildings and infrastructures. Over time, though, many more of these changes will have negative consequences for people and society (Melillo *et al.*, 2014).

One of the important ways to track and reveal the causes and effects of climate change is through indicators (Figure 1). An indicator represents the state or trend of certain environmental or societal condition over a given area and a specified period of time. Collectively, the trends depicted in these indicators provide important evidence of "how climate change looks like" (Environmental Protection Agency, 2016).

There are six major groups of the Indicators: Greenhouse Gases, Weather and Climate, Oceans, Snow and Ice, Health and Society, and Ecosystems. These big groups contain more specific indicators. For example, the ocean group, contain more than five specific indicators: Ocean Heat, Sea Surface Temperature, Sea Level, Coastal Flooding and

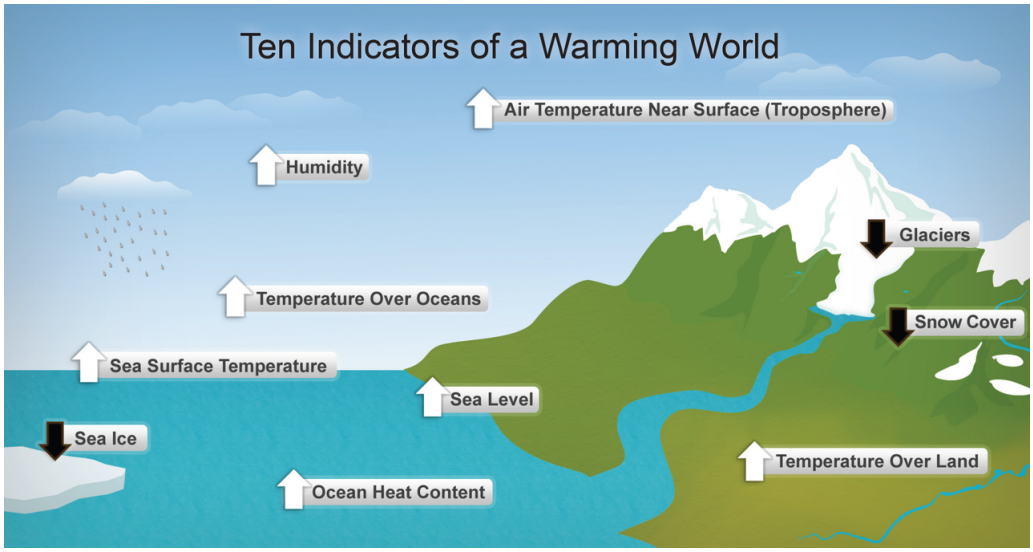

Figure 1: Some climate changes indicators. Source: https://www.climateemergencyinstitute.com/heating.html

Ocean Acidity. The focus of this work will be on the Ocean group indicator, more specifically in the Sea Surface Temperature (SST), which describes trends in the amount of heat stored in the world's oceans.

Nowadays, the Oceans are one of the principal resources of the world. However, they are very complex dynamic systems, which require highly complex multidisciplinary studies to understand their evolution. By the fact that world system has the present characteristics, Oceans have an intrisic environmental, biological, geological or economic value.

Covering about 70% of the Earth's surface, the world's oceans have a cooperative relationship with weather and climate. The oceans influence the weather on local to global scales, while changes in climate can fundamentally reshape many properties of the oceans.

When sunlight reaches the Earth's surface, the world's oceans absorb this energy as heat, which currents distribute around the world. Water has a much higher heat capacity than air, meaning that oceans can absorb large amounts of heat with only a slight increase in temperature. As result, increasing concentrations of heat-trapping greenhouse gases have not caused the oceans to warm as much as the atmosphere, even though they have absorbed more than 90% of the Earth's extra heat since 1955 (IPCC, 2014; Levitus *et al.*, 2012). The large heat-storage capacity of the oceans permit that atmosphere grow warmer more slowly (Levitus *et al.*, 2012). Water temperature reflects the amount of heat in the water at a particular time and location, and plays an important role in the Earth's climate system, because heat from ocean surface waters provides energy for storms, influences weather patterns, and can change oceans currents. Because water expands slightly as it gets warmer, an increase in oceans heat content will also increase the volume of water in the ocean, which is one of the causes of the observed sea level rise.

SST changes are one of the most important sources of uncertainty in future climate changes (Good *et al.*, 2008). SST have important local and remote influences on the global climate through the distribution and transport of heat and moisture. Variations in global and regional SST patterns influence zonal and meridional circulations, which in turn affect the precipitation and temperature patterns across the globe (Bjerknes, 1969; Hastenrath, 1978; Folland *et al.*, 1986; Rodwell *et al.*, 1999; Chang *et al.*, 2000). Changes in ocean circulation patterns modify the warm and cold water transport patterns around the globe, affecting which species are represented in marine ecosystems, altering migration and breeding patterns, threatening corals, and changing the frequency and intensity of harmful algal blooms (Ostrander *et al.*, 2000). Over the

long term, increases in SST could decline the circulation patterns that bring nutrients from the deep sea to surface waters, contributing to decline fish populations, that will affect people who depends on fishing for food or jobs (Pratchett *et al.*, 2004). Higher SST causes an increase in atmospheric water vapor, which increases the risk of heavy rain and snow (IPCC, 2014). Changes in SST can also shift storms tracks, potentially contributing to droughts in some areas (IPCC, 2014).

The general warming of ocean is also an important process to consider when analyzing SAT and other atmospheric physics properties or when investigating the dynamics controlling upwelling (one of the most valuable systems in the oceans).

Although the oceans help to reduce climate change effects by storing large amounts of carbon dioxide, increasing levels of dissolved carbon are changing the chemistry of seawater, turning it more acid. The increase of oceans acidity create problems for certain organisms, such as corals and shellfish, because under this higher acidity in ocean water, these organisms will have difficulties to build their skeletons and shells.These effects could substantially alter the biodiversity and productivity of ocean ecosystems.

To contribute to the study and characterization of SST changes in global warming context, this work aims to assess the worldwide and regional evolution of SST under Climate Change. In order to complement this aim, the following subgoals were defined:

- Evaluation and validation of SST data predicted by GCMs;
- Assessment of SST changes taking into account global warming effects.

1.2 Literature review

All the studies analysed in this section provide insights on evolution of worldwide SST. In this work, special attention was given to characterize and understand the worldwide regionalization of SST and their evaluation under climate change context.

Changes in the ocean are especially important due to its high thermal inertia. In this sense, several studies have reported an increase in the SST (Cane *et al.*, 1997; Levitus *et al.*, 2000, 2005; Mikaloff Fletcher *et al.*, 2006; Harrison & Carson, 2007; Belkin, 2009; Hansen *et al.*, 2010; Levitus *et al.*, 2012; Lima & Wethey, 2012). Levitus *et al.* (2000) found an increase in the heat content of the world ocean around 2×10^{23} Joules between mid-1950 and mid-1990, representing a warming of 0.06 °C. Using data from the U.K. Meteorological Office Hadley Centre climatology from 1957 to 2006, Belkin (2009) found that most of the worldwide coasts are warming, especially in the

Subarctic Gyre, in the European Seas and in the East Asian Seas. Studies with daily SST Analysis provided by Optimum Interpolation Sea Surface Temperature (OISST) 1/4 database were also performed. These Studies found that more than 71% of the world's coastlines have warmed over the period 1982-2010 (Lima & Wethey, 2012; Rodríguez, 2017). However, this warming is far from being homogeneous.

The heterogeneity of the warming trends has led to numerous studies at regional scale (Yoon *et al.*, 2012; Bao & Ren, 2014; Xu *et al.*, 2015; Bouali *et al.*, 2017). However, in earlier stated global studies, Bony *et al.* (1996) used two independent sets of meteorological reanalyses data in order to investigate the relationships between the tropical SST and the large-scale vertical motion of the atmosphere for seasonal and spatial variations between 1987 and 1988. This work concluded that in large-scale subsidence regimes, regardless of the SST range, the cloudiness, the cloud optical thickness, and the shortwave cloud forcing decrease with increasing SST. In convective regions maintained by the large-scale circulation, the strong dependence of both the longwave and shortwave cloud forcing on SST mainly results from changes in the large-scale vertical motion accompanying the SST changes. Indeed, for a given large-scale rising motion, the cloud optical thickness decreases with SST, and the shortwave cloud forcing remains essentially unaffected by SST changes. However, the longwave cloud forcing still increases with SST because the detrainment height of deep convection, and thus the cloud-top altitude tend to increase with SST.

Yoon *et al.* (2012)and Bao & Ren (2014) used monthly SST data from the Met Office Hadley Center's sea ice and sea surface temperature (HadISST) on the periods from 1950 to 2007 and between 1870 and 2011, respectively. Yoon *et al.* (2012) examined the physical processes to the response of SST in the western North Pacific under influence two different types of El Niño (NINO3 and NINO4). Their results suggest that the physical processes, which are responsible for the western North Pacific SST under influence the two different types of El Niño are similar. The results of Bao & Ren (2014) showed that the warming trends of the marginal seas of China during the period from 1870 to 2011 are generally larger than the global and hemispheric averages.

SST changes on Atlantic Ocean were also studied. Xu *et al.* (2015) used OISST version 2 SST dataset with horizontal resolution of $0.25° \times 0.25°$ between 1982 and 2010 in order to study the impacts of the North Atlantic Oscillation (NAO) on SST on the Northeast US Continental Shelf. The correlation between NAO and annual mean SST in the Gulf of Maine was found to be significant and negative at a lag of four years. On South Atlantic region and using high resolution synoptic SST images acquired from NASA's MODIS over 12 years (2003 – 2014), Bouali *et al.* (2017) concluded that satellite data do not suggest significant interannual variability or long term changes

in the magnitude of thermal fronts in the South Atlantic Oscilation. The exception is the upwelling regions of Cape Frio Brazil, where SST gradients have increased at an approximate rate of 1% per year since 2003.

All regional studies demonstrate that SST changes have different behaviors according to distinct locations in the same region. In this context, local studies concerning upwelling systems were performed with different satellite SST datasets (Boer *et al.*, 2007; Alvarez *et al.*, 2009, 2010; Nascimento *et al.*, 2011; Santos *et al.*, 2012; Alonso *et al.*, 2015; Goela *et al.*, 2016). All these studies report higher SST offshore than nearshore, and on SST increase. On period from 1967 to 2007 in western Cantabrian coast, Alvarez *et al.* (2009) concluded that the typical SST response time to upwelling systems was estimated to be around 5 days. The differences between coastal and oceanic SST warming rates along the Canary upwelling ecosystems from 1982 to 2010 were studied by Santos *et al.* (2012). The mean SST calculated from 1982 to 2010 shows gradients both in latitude and in longitude. SST increases southward with a latitudinal gradient around 2°C at the oceanic part of the area. At ocean locations, the SST warming shows a latitudinal increase from north, 0.35 °C/dec, to south, 0.65 °C/dec. Barton *et al.* (2013) used two satellite databases (ICOADS and Pathfinder) between 1967 and 2007 and concluded that on Canary current upwelling, SST is increasing near the coast at all latitudes throughout the region at the a rate higher than 0.01 °C/year. On the other hand, annual SST trends along the Canary upwelling system were also calculated by DeCastro *et al.* (2014), verifying a higher warming (~0.2-0.3 °C/dec). Goela *et al.* (2016) studied the SST and upwelling components from the southwest coast of Portugal between 13th January 1988 and 31st December 2013. This SST analysis showed an increase of 0.15 °C/dec. More recently, Rodríguez (2017) also analysed several upwelling systems (nearshore and offshore areas) and their influences on SST trends, through historical data and estimated a significant general ocean warming rate higher than 0.2 °C/dec on La Guajira, and lower than 0.2 °C/dec on Java. On Yucatan, SST warming rate ranges between 0.1 °C/dec and 0.2 °C/dec.

As reported by mentioned works, SST changes cause different impacts on coastal environments. Thus, several studies were performed in order to assess future SST changes by SST projections by GCMs.

Firstly, historical SST data produced by GCMs were compared with historical SST observations from third (Gillett *et al.*, 2008; Ting *et al.*, 2013) and fifth (Wang *et al.*, 2014; Chan & Wu, 2015) phase of Coupled Model Intercomparison Project. These studies concluded that GCMs present a good reproducibility of SST data. In this way, studies of SST under climate change were performed using this data. Wang *et al.* (2014) analysed SST predictions from 22 climate models of Coupled Model

Intercomparison Project phase 5 (CMIP5). Annual-mean SST errors (that is, means SST bias for the period from 1900 to 2005) magnitudes can have several variations. Thus, SSTs are clearly too high in the tropical south-eastern Pacific and Atlantic and too low in the equatorial and tropical southwestern Pacific. Chan & Wu (2015) developed a new observational constraint method, called multimodel ensemble pattern regression, to correct the projections of regional climate change by the conventional unweighted multimodel mean. This ensemble pattern regression method extracts the leading modes of historical bias using intermodel EOF analysis, and then builds up the linear correlated modes between historical bias and change bias using multivariant linear regression, and finally estimates the common change bias induced by common historical bias. This method was developed to correct the Tropical Pacific SST change under global warming.

Global SST projections also reported a general warming, although with different magnitudes (Xie *et al.*, 2010; He & Soden, 2016). However, SST trends were not determined in these studies. The evolution of SST under climate change at regional level were studied (Good *et al.*, 2008; Huang, 2015; Huang & Ying, 2015; Khalil *et al.*, 2016). Tropical Pacific region analysis was focused on works of Huang (2015) and Huang & Ying (2015). Based on climatic projections, Huang (2015) studied the seasonal changes in tropical SST under global warming based on the representative concentration pathway 8.5 (RCP8.5) and historical runs using 31 models from CMIP5. The tropical SST changes show three pronounced seasonal patterns: the peak locking to the equator throughout the year and the weaker equatorial changes and stronger hemispheric asymmetric changes in boreal autumn. The magnitude of the seasonal patterns is comparable to the tropical-mean warming and the annual-mean patterns, implying great impacts on global climate changes. Khalil *et al.* (2016) focused on Indo Pacific region between 1982 and 2100. They used 22 climate models of CMIP5 of historical and future experiments of RCP 2.6 scenario and concluded that CMIP5 RCP 2.6 forecasts suggested a future warming rate of 0.004 °C/year until 2100.

In line with regional SST predictions reports, local studies focusing upwelling systems were also performed (Rykaczewski *et al.*, 2015; DeCastro *et al.*, 2016; Sousa *et al.*, 2017a). DeCastro *et al.* (2016) determined SST trends during the summer monsoon (June – August) on Somali coastal upwelling. They considered a multimodel mean of seven GCMs of CMIP5 with horizontal resolution of $1° \times 1°$ between 2006 and 2099, and considered the RCP 4.5 and RCP 8.5 scenarios. This work found a significant coastal SST warming (~ 0.35 °C/dec). Spatial trends projected for October – April and May – August were also computed along the coast of Canary upwelling system over the period 2006 – 2009 through 8 simulations that were carried out with CGMs of CMIP5

for historical and climate periods (Sousa *et al.*, 2017a). The authors concluded that SST trends for October – April show lower rates when compared to May – August along the coast, with values around 0.20 °C/dec. These trends contrast with the warming rates observed for the rest of the area. For May – August the pattern of the SST trend is similar, although higher values are detected near the shore (around 0.25 °C/dec).

All these studies provide insights on evolution of worldwide SST. In this work, the worldwide regionalization of SST and their evaluation under climate change context was performed, in order to give a step forward on this subject.

1.3 Structure of this work

The present study is organized in four chapters. The present section introduces the motivation and aims of this work, including important studies for future SST variability performed using Global and Regional Climate Models forecasts.

The second section presents all methods and databases which are used to choose the best models to use in this work, as well as to assess the future SST variability.

Section 3 includes the presentation of results and their discussion.

Finally, section 4 summarizes the main conclusions, and final remarks of this thesis and enunciates future research suggestions.

2 Methodology

The data description as well as the validation procedure is presented in this section, as well as the methodology applied to fulfill the main aims of this work.

2.1 CMIP5 data and experiments

Monthly ocean SST data from 1850 to 2100 were obtained from 27 simulations carried out with GCM (Table 1) developed for CMIP5 (cmip.llnl.gov/cmip5/data_portal.html).

Historical SST data was extracted from the historical run that covers the period 1850 – 2005. The historical run was forced by the observed ocean and atmospheric changes, both from anthropogenic and natural sources (Taylor *et al.*, 2012).

Future SST data was taken for two RCP future climate projections: RCP 8.5 and RCP 4.5, which exhibit a radiative forcing of 8.5 and 4.5 Wm^{-2}, respectively, at the end of the twenty-first century (Moss *et al.*, 2010). For both RCPs the considered period ranged from 2006 to 2100. The 27 models are ensemble models with the r1ip1 initialization, except EC-Earth ensemble model that represents the r6ip1 initialization. Both have the same initialization method indicator, the same perturbed physics, but different realistic initial conditions.

Since the CMIP5 GCMs have different horizontal resolutions (Table 1), SST data were interpolated on a common $1°\times1°$ grid using the nearest neighbor interpolation method.

2.2 Models selection and data validation

An assessment of the performance of GCMs of CMIP5 SST data ensembling to the worldwide SST was carried out, in order to identify the climate models that best reproduce the worldwide SST patterns. In this sense, a comparative analysis between SST data predicted by CGMs of CMIP5 and SST monthly means of daily means data from Era Interim reanalysis (https://www.ecmwf.int/en/forecasts/datasets/archive-datasets/reanalysis-datasets/era-interim) was performed. The comparison was done for the period covering 1979 – 2005.

The data assimilation system used to produce Era Interim data is based on the version 3.0 of NEMO ocean model and the NEMOVAR data assimilation system. The NEMO ocean model spatial discretisation is the tripolar ORCA1 configuration of NEMO, which has a horizontal resolution of around 1°, with equatorial refinement. It uses 42 levels in the vertical, 18 of which are in the upper 200 m.

Table 1: Main Caracteristics of the GCMs of CMIP5 project.

Model	Modeling center	Coupled Ocean Model	Horizontal Resolution (Lon× Lat)
ACCESS1-0	Commonwealth Scientific and Industrial Research Organization (CSIRO) and Bureau of Meteorology (BOM), Australia	MOM4p1	1.1467°× 0.9303°
ACCESS1-3			
CanESM2	Canadian Centre for Climate Modelling and Analysis (CCCMA), Canada	CanOM4	1.41°× 0.94°
CCSM4	National Center for Atmospheric Research (NCAR), USA	POP2	1° × 1°
CMCC-CM	Centro Euro-Mediterraneo per I Cambiamenti Climatici, Italy	OPA8.2	~2°× ~2°
CMCC-CMS			
CNRM-CM5	Centre National de Recherches Météorologiques / Centre Européen de Recherche et Formation Avancée en Calcul Scientifique (CNRM - CERFACS), France	NEMOv3.3	~1°× ~1°
CSIRO-Mk3-6-0	Commonwealth Scientific and Industrial Research Organization in collaboration with Queensland Climate Change Centre of Excellence (CSIRO - QCCCE), Australia	MOM2.2	1.875° × ~0.9375°
EC-EARTH	EC-EARTH consortium (EC-EARTH)	NEMO3.6	~1° × ~1°
GISS-E2-H	NASA Goddard Institute fr Space Studies (NASA GISS), USA	HYCOM	1° × 1°
GISS-E2-H-CC			
GISS-E2-R		Russel	1.25° × 1°
HadGEM2-AO	Met Office Hadley Centre (additional HadGEM2-ES realizations contributed by Instituto Nacional de Pesquisas Espaciais) (MOHC (additional realizations by INPE), United Kingdom	HadGOM2	1°× (1° - 0.3°)
HadGEM2-CC			
HadGEM2-ES			
INMCM4	Institute for Numerical Mathematics (INM), Russia	INMOM	1° × 0.5°
IPSL-CM5A-LR	Institut Pierre-Simon Laplace (IPSL), France	NEMO2.3	~2° × ~2°
IPSL-CM5A-MR			
IPSL-CM5B-LR			
MIROC5	Atmosphere and Ocean Research Institute (The University of Tokyo), National Institute for Environmental Studies, and Japan Agency for Marine-Earth Science and Technology (MIROC), Japan	COCO4.5	1.4063° × 0.5°
MIROC-ESM	Japan Agency for Marine-Earth Science and Technology, Atmosphere and Ocean Research Institute (The University of Tokyo), and National Institute for Environmental Studies (MIROC), Japan	COCO3.4	1.4063° × ~0.9375°
MIROC-ESM-CHEM			
MPI-ESM-LR	Max-Planck-Institut für Meteorologie (MPI-M), Germany	MPIOM	1.5° × 1.5°
MPI-ESM-MR			0.4°× 0.4°
MRI-CGCM3	Meteorological Research Institute (MRI), Japan	MEICOM3	1° × 0.5°
NorEMS1-M	Norwegian Climate Centre (NCC), Norway	MICOM	1° × ~0.5°
NorESM1-ME			

2.2.1 Worldwide SST data division

An attempt to divide the ocean areas of the globe into a manageable number of regions, each with simple shape and a different climatic regime was done. With this purpose, a temporal K-means cluster analysis (Macqueen, 1967) was performed on the climatology created from Era Interim SST data, resulting in a spatial subdivision of the domain in regions with similar temporal behavior (magnitude and variability). Additionally, historical SST data of different GCMs were divided following the same subdivision obtained for Era Interim SST data (DeGaetano & Shulman, 1990; Fovell & Fovell, 1993; Molteni *et al.*, 1996; Legg *et al.*, 2002).

The goal of clustering is to capture the natural structure of the data. This methodology was proposed by Marta-Almeida *et al.* (2016) and Carvalho *et al.* (2016), being applied on atmospheric properties (air temperature and precipitation). K-means cluster analysis is a non-hierarchical clustering method which starts by computing the centroids for each cluster and then calculates the distances between the current data vector and each of the centroids, assigning the vector to the cluster whose centroid is closest to it (Marta-Almeida *et al.*, 2016). Since this is a dynamic method, meaning that vectors can change cluster after being assigned to it, this process is repeated until all vectors are assigned to a cluster (Wilks, 2006).

2.2.2 Comparison between predictions and observations

For validation purposes and in order to select the best model, the historical SST data from different GCMs and observations were compared by two statistical methods: Gaussian Kernel Density Estimator and Taylor Diagrams.

The probability density function was calculated using a Gaussian Kernel Density Estimator (Rosenblatt, 1956; Parzen, 1962) with a default bandwidth. The application of kernel smoothing to the frequency distribution of a data set produces the Kernel density estimate, which is a nonparametric alternative to the fitting of a parametric probability density function. Kernel density smoothing proceeds in an analogous way, using characteristic shapes called kernels, that are generally smoother than rectangles. Table 2 lists four commonly used smoothing kernels, and Figure 2 shows their shapes graphically. Some kernels appropriate to discrete data (able to take on only a finite number of values) are presented in Rajagopalan *et al.* (1997). The argument within the kernel function indicates that each of the kernels employed in the smoothing is centered at its respective data value to each domain.

Table 2: Common smoothing kernels (Wilks, 2006).

Name	K(t)	Support [t for which K(t)>0]	$1/\sigma_k$
Triangular	$1 - \|t\|$	$-1 < t < 1$	$\sqrt{6}$
Quadratic (Epanechnikov)	$(3/4) - (1 - t^2)$	$-1 < t < 1$	$\sqrt{5}$
Quartic (Biweight)	$(15/16)(1 - t^2)^2$	$-1 < t < 1$	$\sqrt{7}$
Gaussian	$(2\pi)^{-1/2} exp[-t^2/2]$	$-\infty$<t<∞	1

This approach was applied for each region defined with cluster analysis in order to compare all models performance using Era Interim data as reference.

To compare the probability distributions of the observed and predicted variables, the Kolmogorov-Smirnov test was performed (*KS*-test, Kolmogorov, 1933; Smirnov, 1948). This test is robust to outliers, just like the other commonly used Mann-Whitney test (MW-test, Whitney & Mann, 1947), but is more robust to detected changes in the shape of the distribution than the MW-test(Lehmann, 2006).

In addition, the adjustment between SST from different GCMs CMIP5 and Era Interim database was quantified through Taylor Diagrams. These diagrams allow three different measures of uncertainty, Standard Deviation (*SD*), Correlation (*Co*) and Root Mean Square Deviation (*RMSD*). To be considered simultaneously, Taylor Diagram parameters (*SD*, *Co*, and *RMSD*) were performed according to following equations (Eq. 1, Eq. 2 and Eq. 3 respectively).

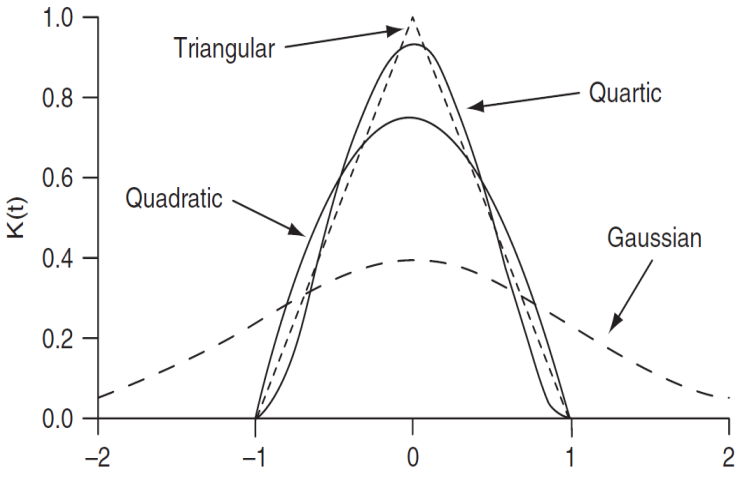

Figure 2: Shapes of common smoothing kernels (Wilks, 2006).

$$SD = \sqrt{\frac{\sum_{i=1}^{N} (C_i - c_i)^2}{N}} \tag{1}$$

$$RMSD = \sqrt{\frac{\sum_{i=1}^{N} \left([(C_i - c_i) - (C_{r_i} - c_{r_i})]^2 \right)}{N}} \tag{2}$$

$$Co = \frac{\sum_{i=1}^{N} ([C_i - c_i] \times [C_{r_i} - c_{r_i}])}{N \times SD\,(C) \times SD\,(C_{r_i})} \tag{3}$$

where C are model predictions, C_r is Era Interim data, N is the number of data points, and c and c_r are the average of C and C_r, respectively.

A diagram has been drawn to provide a concise statistical summary of how well patterns match each other in terms of their *Co*, *RMSD*, and *SD*. Although the form of this diagram is general, it is especially useful in evaluating complex models, such as those used to study geophysical phenomena. Taylor Diagram method is suggested for indicating the statistical significance of apparent differences and the degree of agreement between GCMs of CMIP5 and Era Interim data (Taylor, 2001).

To accomplish the taylor diagram analysis, RMSD and normalized Co (η) were used like quantitative statistical measures, referred to as performance metrics (Me). The use of such metrics simplifies synthesis and visualization of model performance (Gleckler *et al.*, 2008; Pincus *et al.*, 2008; Waugh & Eyring, 2008; Cadule *et al.*, 2010; Sahany *et al.*, 2014) and enables the quantitative assessment of model improvements over time (Reichler & Kim, 2008). Recent work has addressed redundancy of multiple performance metrics through methods such as cluster analysis (Yokoi *et al.*, 2011; Nishii *et al.*, 2012).

Normalized Co and Me were calculated by equations 4, and 5, respectively.

$$\eta = |1 - Co| \tag{4}$$

$$Me = \frac{1}{N_m} \sum_{i=1}^{N_m} M_i \tag{5}$$

where N_m is the number of metrics and M is the metrics (η and *RMSD*). Thus, results of all statistical methods allowed selecting a group of better representing models.

2.3 Climate change impacts in future SST variability

Data from the selected climate models was used to assess global future SST changes in the selected regions. Extracted data from the GCMs were organized in a multimodel mean in order to minimize the individual biases (Räisänen & Palmer, 2001; Van Oldenborgh *et al.*, 2013; Rykaczewski *et al.*, 2015; Sousa *et al.*, 2017a; Sousa *et al.*, 2017b).

To assess SST differences between the historical period (1975 -2005) and each RCP climatic scenario, different study climate regimes were created, being the future period divided into two study regimes, a near future (2020 – 2050) and a long-term future (2070- 2100) (Table 3).

Inter-annual averages of monthly means were calculated for each region and regime. Additionally, differences among these averages were calculated on each domain in order to identify the higher monthly differences. Global variations between historical period and the two futures were evaluated by percentual variation differences. The percentual variation was calculated according to following equation (Eq. 7):

$$\triangle SST(\%)_{(i,j)} = \frac{SST_{f_{(i,j)}} - SST_{p_{(i,j)}}}{SST_{p_{(i,j)}}} \times 100 \tag{6}$$

where i is latitude points, j is longitude points, SST_f is future SST data and SST_p is recent-past SST data.

Following the methodology adopted by Tebaldi *et al.* (2011), Wang *et al.* (2015) and Sousa *et al.* (2017a), SST trends (1975 - 2100) were calculated for each region and pixel as the slope of the linear regression. The latitudinal and longitudinal average of multimodel mean (1975 - 2100) were performed in order to calculate the trends in each region. The robustness of multimodel mean spatial projections was also evaluated by applying the paired Student's *t test* (Press *et al.*, 1992), which identify the locations of statically significant differences (*p-values* lower than 0.05) between future and historical periods.

Table 3: Study Climate Regimes.

Regimes	Historical	F1RCP4.5	F1RCP8.5	F2RCP4.5	F2RCP8.5
Time (Years)	1975 - 2005	2020 - 2050		2070 - 2100	

3 Results and Discussion

The characterization of SST changes in global warming context are presented in this section, which is divided in three subsections. The first one shows the worldwide SST division results. Posteriorly, an assessment of models predictions and their validation results are presented in second part of this section. The last one presents the results of climate change impacts in future SST variability.

3.1 Worldwide SST data division

In order to identify the worldwide regions with consistent SST changes (magnitude and variability), kmeans results of Era Interim reanalysis SST data were analyzed (Figure 3). Analysing gap values demonstrates that SST data can be divided into a different number of regions, ranging from one to nine groups. The optimed number of clusters (k) as determined by this method corresponds to the first local minimum, in this case when gap values of data are nearly constant. This condition was verified when k is comprehended between 1 and 7.

When applying the clustering algorithm to SST data using k value of 3 (Figure 4), the domain is divided into three regions for each hemisphere. The Polar and Sub-Tropical regions cannot be divided with this number of clusters and these two regions present significant SST differences between them. When the number of clusters is increased, more regions to each hemisphere can be observed and therefore the regions obtained

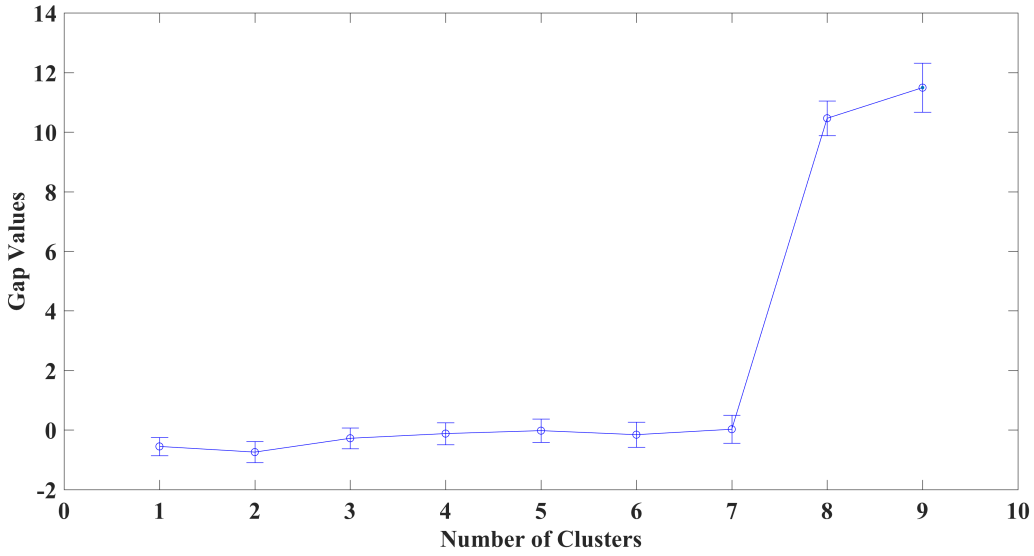

Figure 3: Gap values of climatology of Era Interim data.

will provide a more detailed definition of the changes (Carvalho *et al.*, 2016).

Applying the clustering algorithm to SST data using k=4, the domain is divided into four regions for each hemisphere. With this division, the Equatorial and Tropical regions remains like in previous division, nevertheless the Polar and Sub-Tropical regions can be divided. For k=5, 6 and 7, the clustering algorithm also generated new regions between previous defined regions (k=4). Considering the main aim of this work, these new regions do not present physical significance. Thus, it can be concluded that k=4 better fits this work purposes. Consequently, the worldwide SST data is divided into eight regions: Polar Region (PRN – PRS), Sub-Tropical Region (STRN – STRS), Tropical Region (TRN – TRS) and Equatorial Region (ERN – ERS) (Figure 5).

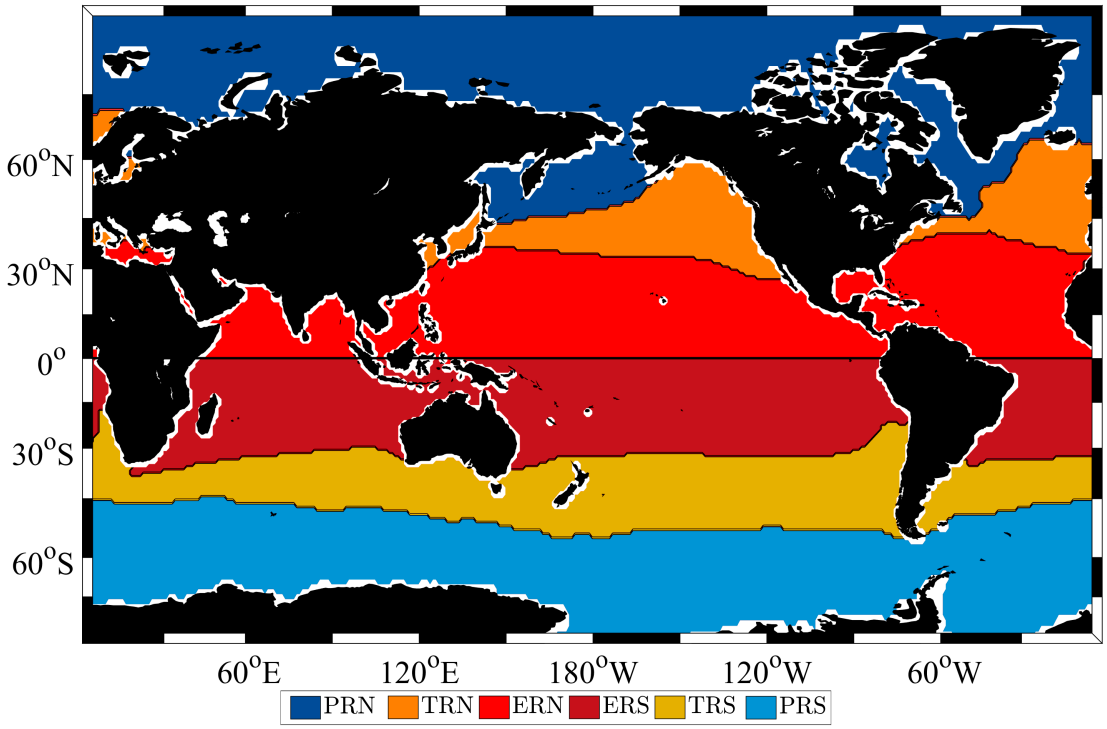

Figure 4: Worldwide regions based on K-means cluster analysis with three clusters. Polar Regions (PRN – PRS), Tropical Regions (TRN – TRS) and Equatorial Regions (ERN – ERS).

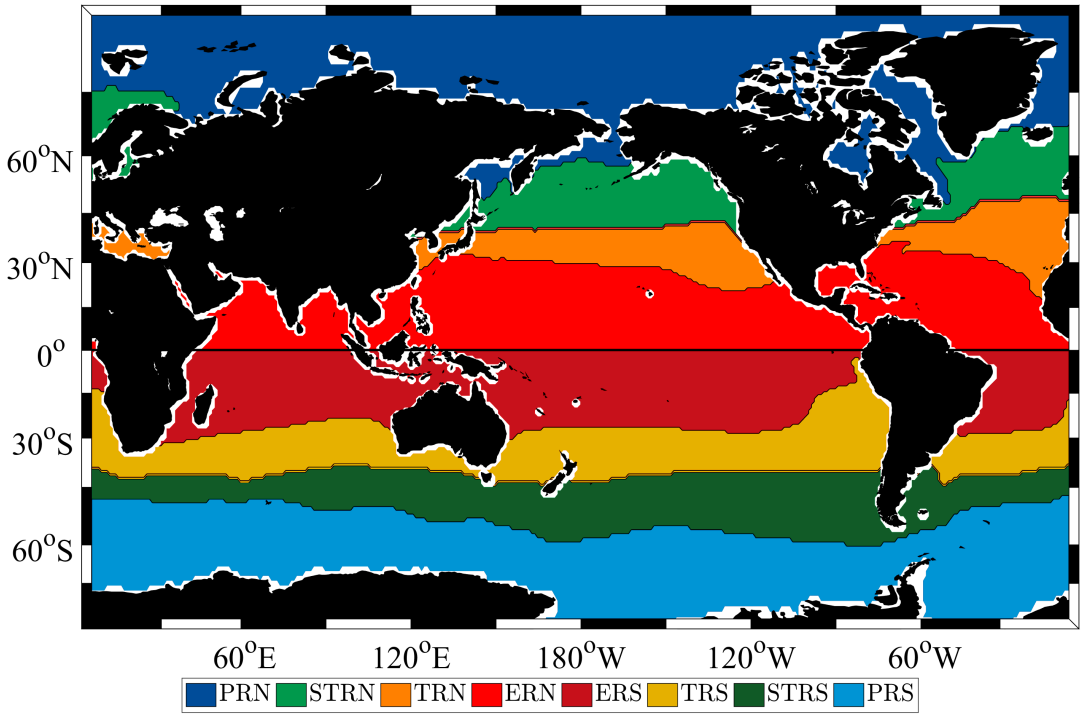

Figure 5: Worldwide regions based on K-Means cluster analysis with four clusters. Polar Regions (PRN – PRS), Sub-Tropical Regions (STRN – STRS), Tropical Regions (TRN – TRS) and Equatorial Regions (ERN – ERS).

3.2 Comparison between predictions and observations

The validation of SST predictions from GCMs of CMIP5 to each region is made by comparing the models predictions with Era Interim data for the same regions. This comparison was performed by Gaussian Kernel Density Estimator, KS-test, Taylor Diagram and associate metrics.

The comparison resulting from the Kernel Density Estimator is shown in Figure 6. The Kernel Density distribution results are organized so that each column corresponds to each Hemisphere: North (left) and South (right), and the rows correspond to each region: Polar, Sub-Tropical, Tropical and equatorial (top to bottom, respectively).

The results for Kernel Density distribution show a similar pattern between SST predictions from GCMs of CMIP5 and Era Interim data for all clusters, except for the PRN domain where SST predicted by two models (MPI-ESM-LR and MPI-ESM-MR) has a different distribution. SSTs simulated by CMIP5 models generally show low values in the North Hemisphere and high values in the South Hemisphere. As expected, SST values increase from Poles to the Equator. Global minimum SST occurs in poles (-4 °C), with a probability density of 0.5 for the South Pole and 0.42 for the North Pole.

Global maximum SST occurs in Equator (about 27.5 °C), with a probability density of 0.3.

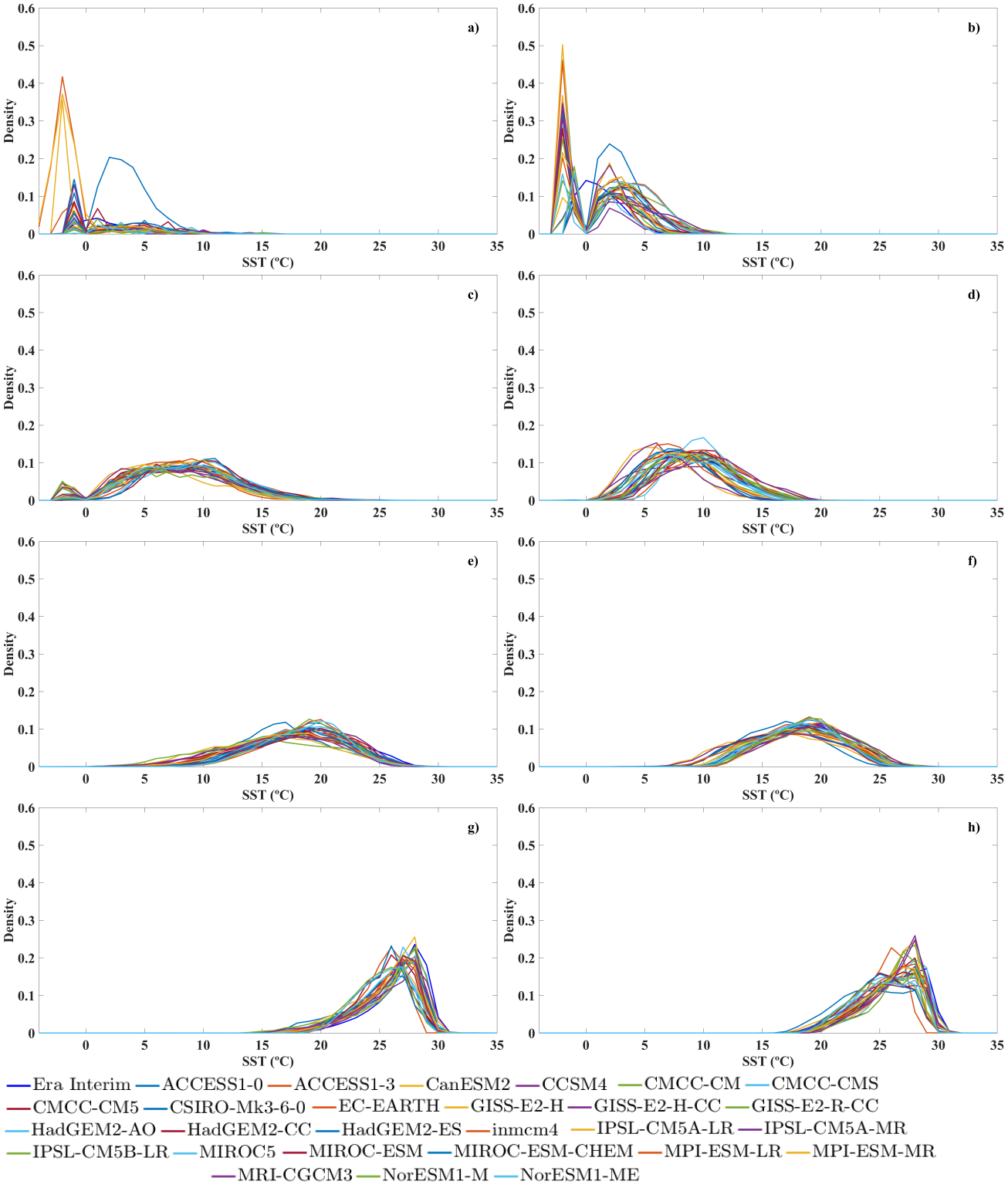

Figure 6: Kernel Density Estimator distribution for each region: (a) PRN, (b) PRS, (c) STRN, (d) STRS, (e) TRN, (f) TRS, (g) EQN and (h) EQS.

In order to compare the probability distributions of the predicted and observed SST data, resulting from Kernel Density function, KS-test results are presented in Appendix A. In KS-test, high p-values or low d-values (maximum distance between the cumulative distributions) indicate the null-hypothesis that both groups (models predictions and Era Interim data) were sampled from populations with similar distributions. Thus, with this condition verified the prediction data cannot be rejected.

In all regions, p-values range from 0.5 to 1. According to Marta-Almeida *et al.* (2016), p-values higher than 0.05 (the usual level of significance) indicate that should not be rejected the hypothesis that the sets belong to populations with the same probability distribution. KS-test results are in agreement with the Kernel Density Estimator results (Figure 4), allowing the elimination of the same models.

In order to complement Kernel Density Estimator results, Taylor Diagrams results were analysed, and results depicted in Table 4 and Figure 7. As for Kernel Density Estimator results, Taylor Diagrams have similar SST patterns from GCMs of CMIP5 and Era Interim data. Ideal values of statistical parameters for Taylor Diagrams are 0 °C to *RMSD*, 1 °C to *SD* and 1 to *Co*. Minimum of *RMSD* (0.33 °C) occurs in TRS and maximum occurs in Polar Regions (1.00 °C). The PRS and PRN present the maximum (1.70 °C) and minimum (0.60 °C) values, respectively. Regarding *Co*, maximum value (0.94) occurs in TRS, STRS and PRS, while minimum value (0.30) occurs in PRN.

Figure 7 shows a similar dispersion for all GCMs, except for PRN (Figure 7a) and PRS (Figure 7b) regions, where significant differences between GCMs were found, mainly in PRS region.

In addition, *RMSD*, η and *Me* were analyzed for each region and climate model (Figure 8). As for the previous results regarding Taylor Diagram (Figure 7 and Table 4), the PRS presents worse results in *RMSD*, η and *Me* parameters. Since SST data horizontal resolution from GCMs of CMIP5 decreases from equator to poles, it was expected that Taylor Diagrams results would not have ideal values for statistical parameters on polar regions. For Sub-Tropical, Tropical and Equatorial regions, GCMs SST show consistent and convergent results with majority of climate models, presenting *Me* values lower than 0.5 °C.

Large-scale performance metrics are a typical first-step to quantify model predictions agreement with observations and summarizing broad characteristics of models performance that are not focused on a particular application. *Me* values lower than 0.5 °C were considered as a good model prediction agreement with observations, whereas *Me* values higher than 0.5 °C represent a poor model performance. Following this criterion, CSIRO-Mk3-6-0, IPSL-CM5B-LR, and MRI-CGCM3 models had a lower agreement

with SST data observations.

Several reports about climate change effects on SST predictions from CGMs of CMIP5, used numerous climate models, mainly MPI-ESM-MR and MPI-ESM-LR models (Huang, 2015; Huang & Ying, 2015; Chan & Wu, 2015). Nevertheless, these reports do not focus on polar regions, but rather in restricted latitudes. In this work and considering the Kernel Density Estimator and metrics results, five models were rejected: CSIRO-Mk3-6-0, IPSL-CM5B-LR, MPI-ESM-MR, MPI-ESM-LR, and MRI-CGCM3. Thus, in the next section, predictions from these models were not considered in the analysis of the future changes in the worldwide and regional SST under climate change. Henceforward, in order to minimize the individual biases, a multimodel mean of SST predictions from 22 models will be considered to analyze the global future

Table 4: Minimum and maximum values of Taylor Diagrams variables for each reagion.

Regions	*RSMD* (°C)	*SD* (°C)	*Co*
PRN	0.50 - 1.00	0.60 - 1.00	0.30 - <0.90
STRN	0.42 - 0.90	0.90 - 1.25	0.71 - 0.93
TRN	0.39 - 0.79	0.82 - 1.30	0.81 - 0.93
ERN	0.40 - 0.72	0.90 - 1.32	0.81 - 0.93
ERS	0.41 - 0.61	0.85 - 1.20	0.81 - 0.93
TRS	0.33 - 0.55	0.92 - 1.25	0.85 - 0.94
STRS	0.40- 0.58	0.80 - 1.30	0.85 - 0.94
PRS	0.38 - 1.00	0.98 - 1.70	0.75 - 0.94

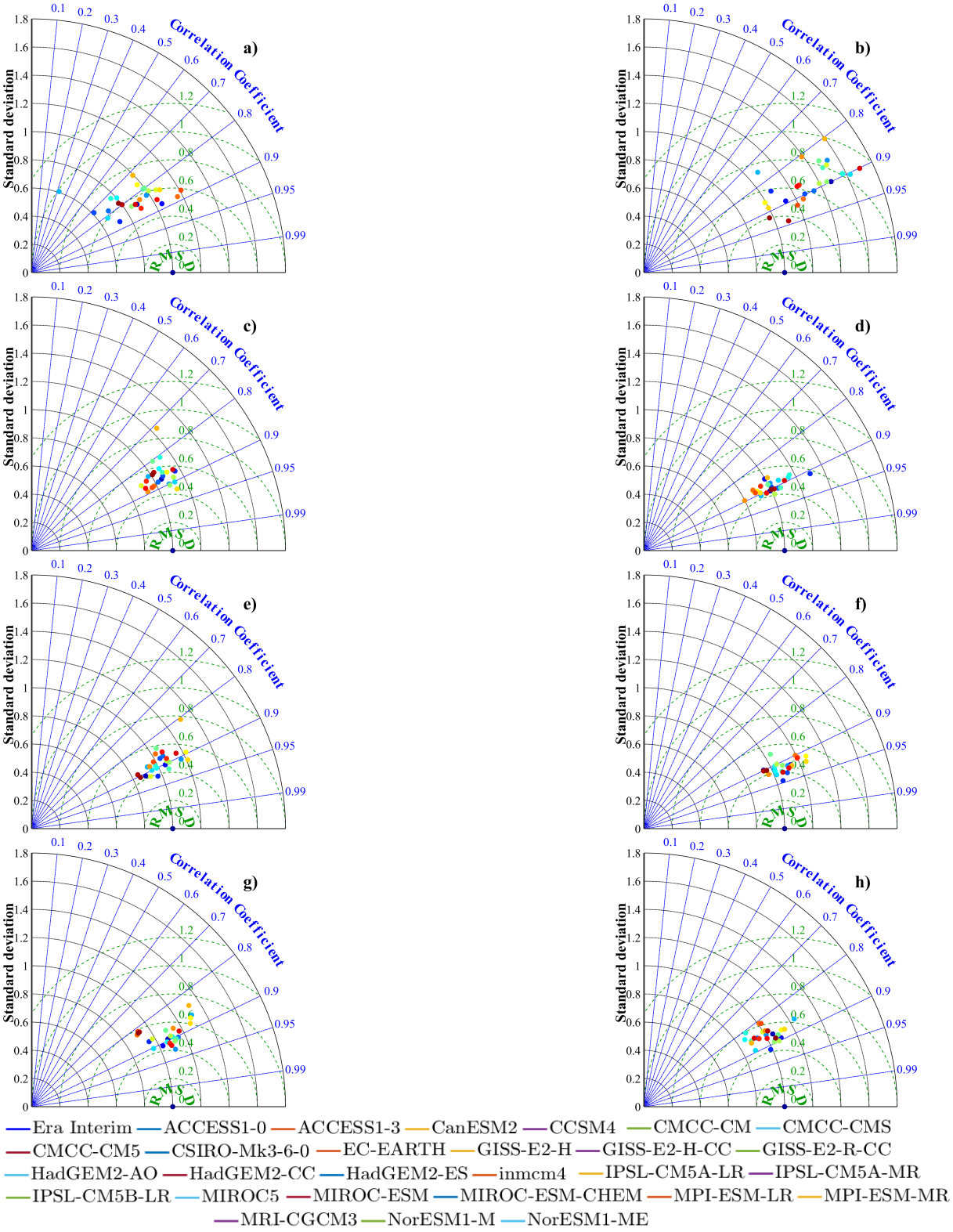

Figure 7: Taylor Diagrams comparing SST data from Era Interim and from different GCMs of CMIP5 predictions for each region: (a) PRN, (b) PRS, (c) STRN, (d) STRS, (e) TRN, (f) TRS, (g) EQN and (h) EQS. Blue, green and black lines correspond to *SD*, *RMSD* and *Co* respectively.

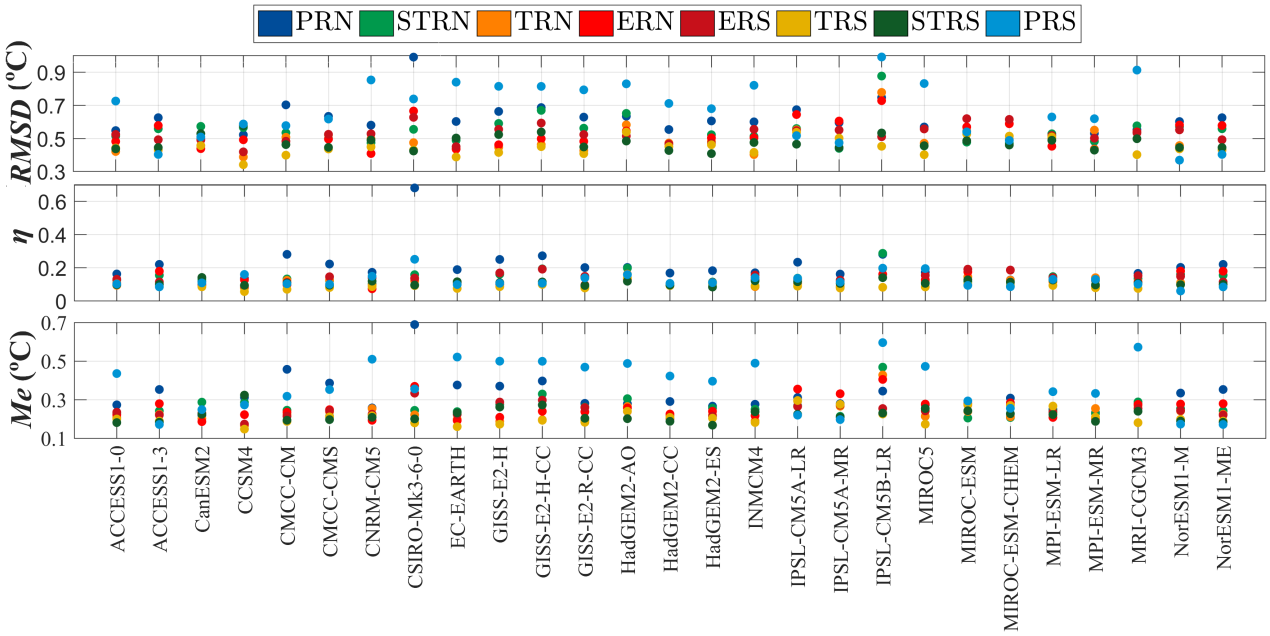

Figure 8: Metrics (*RMSD*, η, *Me*) for all regions and models.

3.3 Climate change impacts in future SST variability

The multimodel SST data mean of selected GCMs was done and organized in inter-annual means of monthly means to each region and regime (Figure 9).

Figure 9 (a, c, e and g) corresponds to North Hemisphere, while the remaining subplots refer to South Hemisphere (Figure 9 b, d, f and h). On both hemispheres, the winter months (lower temperatures) and summer months (higher temperatures) are clearly identified. Thus, SST seasonality of each hemisphere is clearly recognized.

As expected, SST values for RCP 8.5 scenario are higher than for RCP 4.5 scenario in all regions for both periods (2020 – 2050 and 2070 – 2100). Considering the both hemispheres, the north regions present higher thermal amplitude (differences between maximum value of SST in long-term future (2070 - 2100) for RCP 8.5 scenario and minimum value of SST for historical regime), comparing with equivalent regions of south hemisphere. Taking into account all study regimes and regions, in North Hemisphere the SST ranges from -1.5 °C to 32 °C, while in South Hemisphere ranges from 0 °C to 32 °C. For both hemispheres, minimum SST data was found in polar regions for the historical regime (1975 – 2005) and maximum in equatorial regions for a long-term future (2070 – 2100) for RCP 8.5 scenario. As result of the higher thermal amplitude on North Hemisphere, differences between seasons and study regimes are more evident.

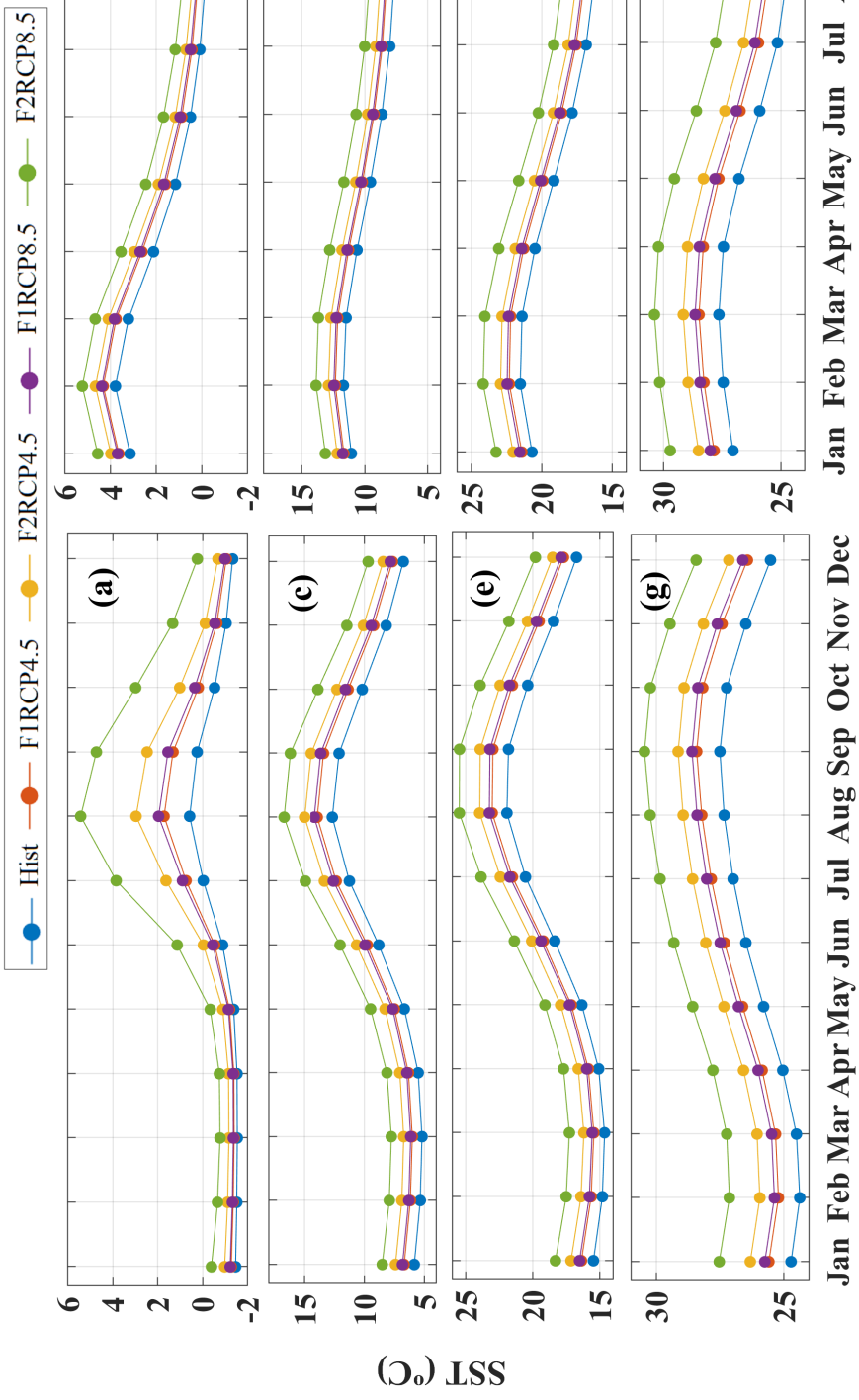

Figure 9: Inter-annual means of monthly means to each region and regime to PRN (a), PRS (b), STRN (c), STRS (d), TRN (e), TRS (f), ERN (g) and ERS (h). Blue line represents historical regime (1975 - 2005), red and yellow lines represent near (2020 - 2050) and long term future (2070 - 2100) for RCP 4.5 scenario, respectively. Purple and green lines represent near (2020 - 2050) and long term future (2070 - 2100) for RCP 8.5 scenario, respectively.

Concerning each region of North Hemisphere, maximum SST of historical regime was found in August on PRN and STRN, in August and September in TRN and in September in ERN. Regarding the near and long-term futures, maximum temperatures similar with the historical regime will be observed between June and July and between September and November to near and long-term futures, respectively, in PRN, STRN, and TRN. On ERN region, the maximum temperatures for the historical regime will occur between May and June, and between October and November for both futures of RCP 4.5 scenario.

The same analysis for RCP 8.5 scenario, shows that the pattern is similar to that described for RCP 4.5 scenario on PRN, STRN, and TRN. On ERN, for the near-term future of RCP 4.5 scenario, the maximum SST for historical regime was found between June and July, and November. For the long-term future, the maximum SST for historical regime on ERN will occur in January, between March and April, and in November. Considering the long-term future obtained for the two RCP scenarios for the south hemisphere, PRS, STRS, TRS, and ERS will have an average lag of maximum SST regarding the historical regime of one, two, three and four months, respectively. For near-term future, this lag will not exceed the two months for all south regions.

To quantify the differences between periods, Figure 10 shows the monthly SST climatological differences between long-term future (2070– 2100) and historical period (1975–2005), and between near-term future (2020 – 2050) and historical period (1975 – 2005) for RCP 8.5 and RCP 4.5 scenarios.

The mean regional monthly SST climatological differences for the eight regions present distinct climatological changes, which vary throughout the seasons in distinct ways. The climatological differences are always positive for all regions and scenarios, indicating a warming of all regions, although varying with different magnitude. The major SST difference will occur between long-term future of RCP 8.5 scenario and historical period, reaching 5 °C in August, while the minimum SST difference will occur between January and May in PRN with similar magnitude for both scenarios. The positive differences indicate that worldwide SST will increase, comparing to the historical period. These results are in agreement with IPCC (2014)forecasts.

Regarding the results for both futures for RCP 4.5 and RCP 8.5 scenarios, similar patterns were found in differences between near-term futures and historical regime (Figure 10 (a)-(c)) and between long-term futures and historical regime (Figure 10 (b)-(d)). The monthly differences between long-term future of RCP 8.5 scenario and the historical regime decrease from North to the South Pole for the third trimester (July, August, and September). For the same period, monthly differences between RCP 4.5

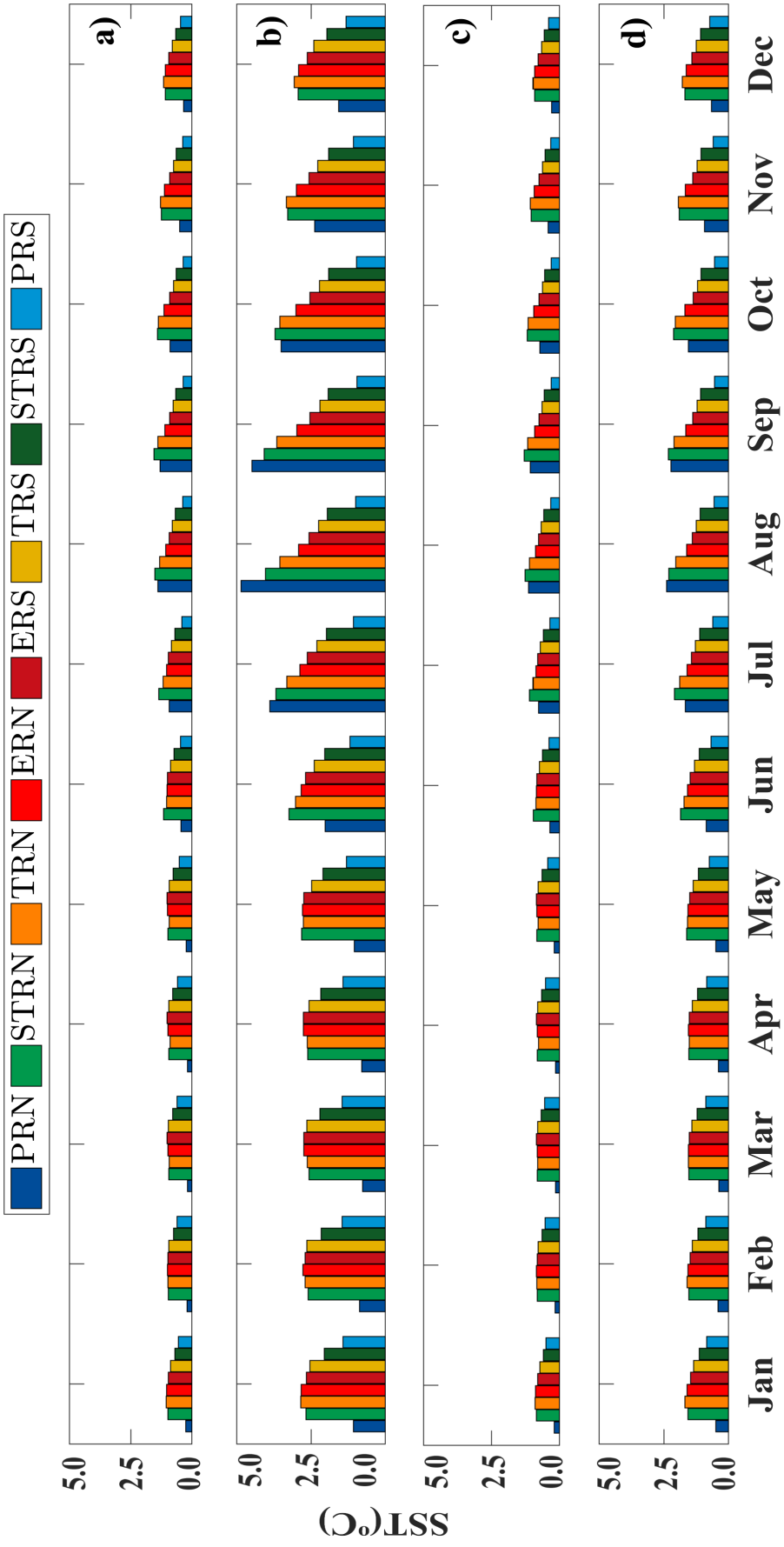

Figure 10: SST annual means of monthly means differences between two futures regimes of RCP scenarios and historical regime (1975 - 2005): (a) RCP 8.5 scenario (2020 - 2050); (b) RCP 8.5 scenario (2100 - 2070); (c) RCP 4.5 scenario (2020 - 2050); (d) RCP 4.5 scenario (2100 - 2070).

scenario and historical regime only will be higher in PRN than in STRN in August.

Considering the period from January to June, the differences between 2070 - 2100 and 1975 – 2005, and between 2020 – 2050 and 1975 – 2005 for RCP 4.5 scenario will not be significant among STRN, TRN, and ERN. Therefore, it is expected that the remaining months will be responsible for global differences among these regions. For RCP 8.5 scenario, with exception of June, the differences show the same pattern.

Regional monthly SST climatological differences mean are shown in Table 6. North Hemisphere has a higher SST increment than South regions. In general, as expected, the differences between long-term future (2070– 2100) and historical regime (1975 – 2005) are larger than differences between near-term future (2020 – 2050) and recent-past. For the long-term future, worldwide SST will have mean increments of 2.46 °C and 1.35 °C for RCP 8.5 and RCP 4.5 scenarios, respectively. Regarding the near-term future, worldwide SST will have mean increments of 0.86 °C and 0.73 °C for RCP 8.5 and RCP 4.5 scenarios, respectively.

Results obtained in this work are in agreement with previous IPCC predictions, which show that ocean surface warming will vary considerably between the emission scenarios, ranging from 1 °C to more than 3 °C (subtropical and tropical regions) (IPCC, 2014).

Depending on regions, SST values increments will have different effects in worldwide SST changes. Thus, Figure 11 shows percentual SST variability between near (2020 – 2050) and long-term (2070 – 2100) future and recent-past (1975 -2005) for RCP4.5

Table 6: Regional SST monthly means differences between RCP scenarios and historical period (1975 - 2005).

Regions	RCP 4.5 scenario		RCP 8.5 scenario	
	Near-term future (2020 - 2050) (°C)	Long-term future (2070 - 2100) (°C)	Near-term future (2020 - 2050) (°C)	Long-term future (2070 - 2100) (°C)
PRN	0.46	1.03	0.57	2.27
STRN	0.99	1.84	1.18	3.19
TRN	0.95	1.79	1.12	3.09
ERN	0.87	1.60	1.04	2.87
ERS	0.80	1.44	0.96	2.64
STRS	0.71	1.30	0.85	2.41
TRS	0.60	1.12	0.71	2.03
PRS	0.41	0.70	0.47	1.22

and RCP 8.5 scenario.

For near-term future and historical period, a similar pattern can be observed between subplots relative to percentual difference (Figure 11a and Figure 11c), although the variability resulting from RCP 8.5 scenario presents a slight percentual increase, mainly in the equatorial region. Taking into account the percentual difference between long-term future and historical period, a similar pattern will be observed in both RCP scenarios, mainly in latitudes of ERS and TRS regions. Globally, averaged SST from CMIP5 models is projected to warm over the 21^{st} century. In general, for all scenarios, the largest warming is found for the high latitudes of North Hemisphere.

The variability associated to a long-term future (2070 – 2100), for RCP 8.5 scenario, will decrease about 0.5% for the the region between Australia and South America and for Indo-Pacific region, comparing with surrounding regions. For RCP 4.5 scenario, the variability will decrease about 0.25%. Regional variations in the projected amplitude of ocean temperature change can be influenced by ocean circulation as well as by surface heating (Timmermann *et al.*, 2007; DiNezio *et al.*, 2009; Yin *et al.*, 2009; Xie *et al.*, 2010; Yin *et al.*, 2010).

For all scenarios, percentual SST variability presents a significant spatial variation in Tropical and Sub-Tropical regions. These variations can be explained by Inter-decadal variability of upper ocean temperatures, which is larger in mid-latitudes, particularly in the North Hemisphere than in the tropics (Wang *et al.*, 2010).

To understand the SST differences evolution on different regions, Figure 12 shows the interannual evolution of SST for each region, ranging from 1975 to 2100 for both RCP scenarios. A significant increasing in SST will occur in all regions and RCP scenarios.

As it can be observed in Figure 12, North regions will present higher thermal amplitudes, which are reflected in upper SST trends. SST trends for RCP 4.5 and RCP 8.5 scenarios for all regions are summarized in Table 7. On North Hemisphere, for RCP 8.5 scenario SST trends will be 4.34 °C (maximum) and 3.44 °C (minimum) for STRN and ERN, respectively. Regarding RCP 4.5 scenario for the same regions, SST trends will be 1.96 °C, 2.64 °C, 2.30 °C, and 2.18 °C from PRN to ERN, respectively. For South Hemisphere, in both scenarios, SST trends will be smoother compared to the North Hemisphere. These results are in line with Santos *et al.* (2012) that obtained a latitudinal gradient around 2 °C at the oceanic part of Canary upwelling system between 1982 and 2010.

Comparing both RCP scenarios, the differences between SST trends for the equivalent regions decrease from North to the South Pole, corroborating the increase of SST on North Hemisphere. Polar and subpolar regions of North Hemisphere present lower SST

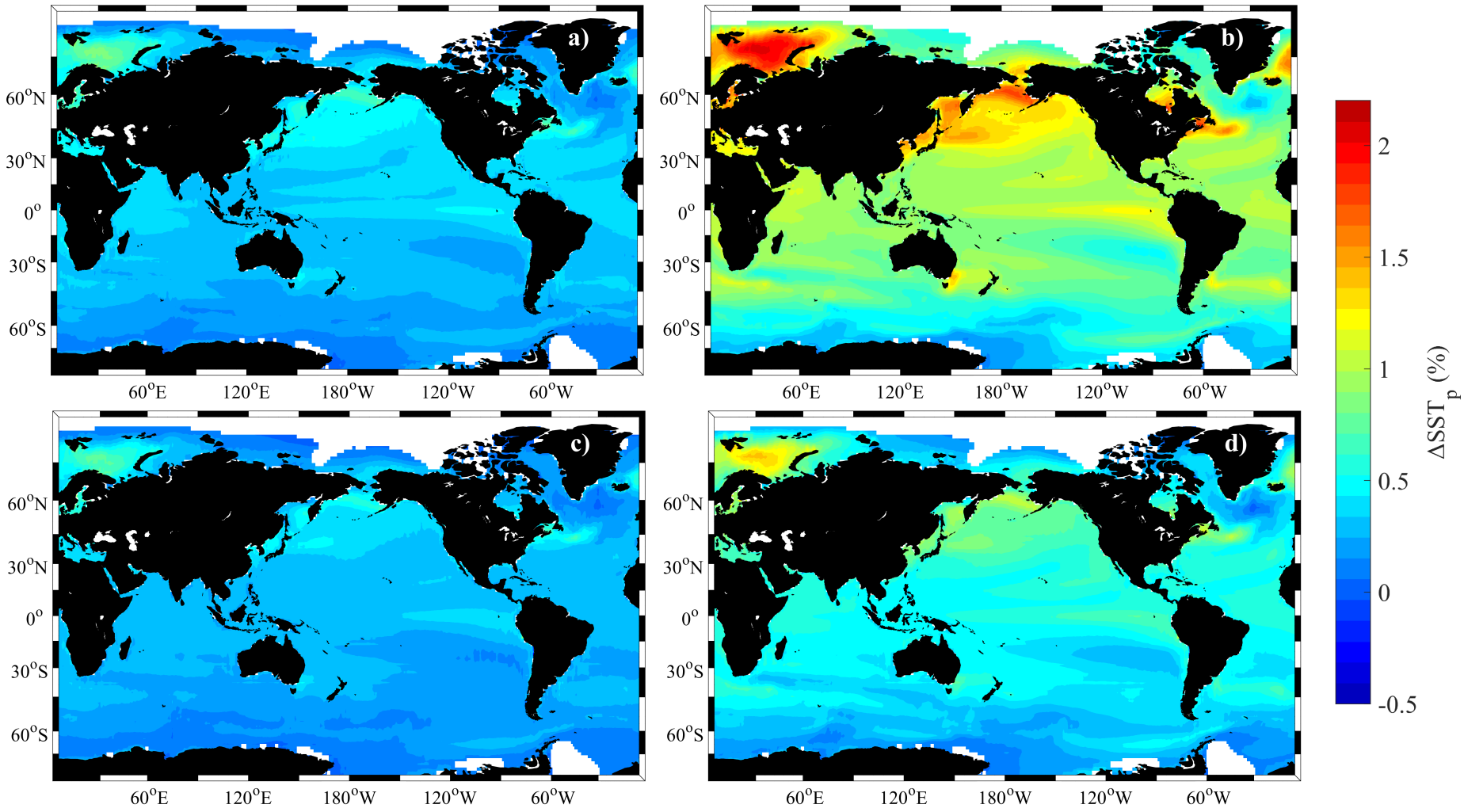

Figure 11: SST percentual variation between RCP scenarios and recent-past (1975 - 2005): (a) RCP 8.5 scenario (2020 - 2050); (b) RCP 8.5 scenario (2100 - 2070); (c) RCP 4.5 scenario (2020 - 2050); (d) RCP 4.5 scenario (2100 - 2070). White areas correespond to the sea ice.

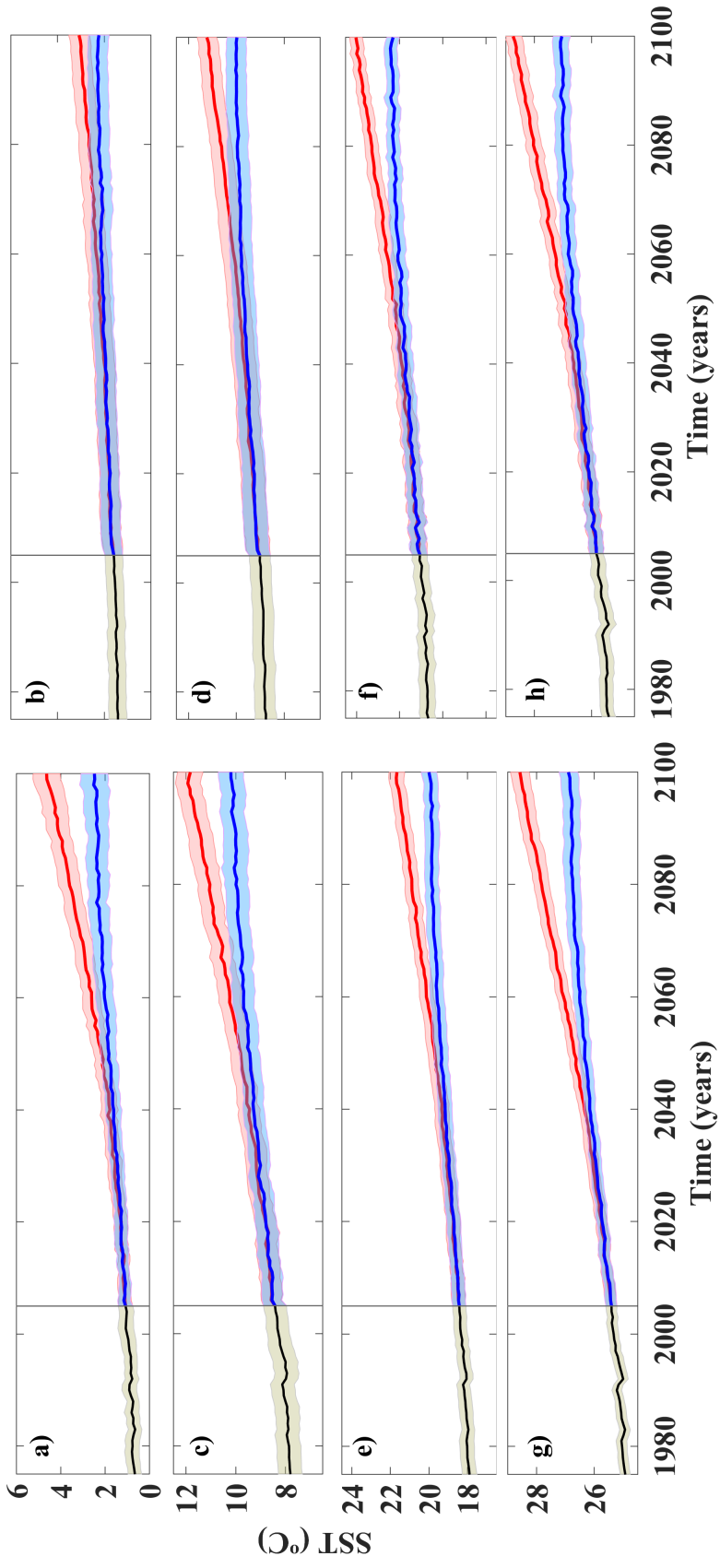

Figure 12: SST trends for each region from 1975 to 2100: PRN (a), PRS (b), STRN (c), STRS (d), TRN (e), TRS (f), ERN (g) and ERS (h). Black line represents historical regime, blue line represents RCP4.5 and red line represents RCP8.5. Shaded areas represent deviations.

values in 1975, than same regions of South Hemisphere. However, for PRN and STRN in the future (2100), SST values will be higher than in PRS and STRS. For equatorial regions, future SST values at end of 21^{st} century will be the same for both scenarios. For tropical regions, future SST values at end of 21^{st} century will be higher in TRS than in TRN. All regions present significant differences between both RCP scenarios ranging from 2020 to 2040, except PRS where significant differences occur between 2040 and 2060.

To better analyze and quantify the SST variability, spatial SST trends were also computed for RCP 4.5 and RCP 8.5 scenarios between 1975 and 2100 (Figure 13). Trends are statistically robust across climate models and are significant in almost all regions, with exception of South Pole and North Atlantic regions.

Overall, a significant worldwide SST warming is projected for both RCP scenarios, although less intense in poles, except near the north of Norway, in North Pole. A general warming along the coast will be also observed, in line with previous studies based on historical SST data, which reported an increasing SST trend during the second half of the last century (Lima & Wethey, 2012; Barton *et al.*, 2013). Both scenarios present higher SST trends in North Hemisphere, namely in Subtropical Region, in agreement with time series results (Figure 12). The maximum SST warming rates will be observed on North Hemisphere for RCP 4.5 (0.5 °C/dec) and RCP 8.5 (0.8 °C/dec) scenarios.

For both RCP scenarios, SST trends in the South Pole vary from 0.1 °C/dec to 0.2 °C/dec, in agreement with regional results obtained in Figure 12. Analyzing trend maps (Figure 13), is found that for more than 50% of points of North Pole trends vary between 0.1 °C/dec and 0.2 °C/dec. However, times series of PRN (Figure 12 a) present the higher SST trends (1.96 °C and 3.86°C) between 1975 and 2100 for RCP 4.5 and RCP 8.5 scenarios, respectively.

The SST changes found in this work are in line with the results obtained by Rodríguez (2017), that analysed several upwelling systems (nearshore and offshore areas) and their influences on SST trends through historical data, and estimated a significant general ocean warming rate higher than 0.2 °C/dec on La Guajira, and lower than 0.2 °C/dec on Java. On Yucatan, SST warming rate ranges between 0.1 °C/dec and 0.2 °C/dec.

Table 7: SST trends for RCP 4.5 and RCP 8.5 scenarios for all regions.

Scenarios	PRN	STRN	TRN	ERN	ERS	TRS	STRS	PRS
RCP 4.5 (°C)	1.96	2.64	2.30	2.18	1.88	1.92	1.41	0.94
RCP 8.5 (°C)	3.86	4.34	3.95	3.84	3.44	3.49	2.52	1.64

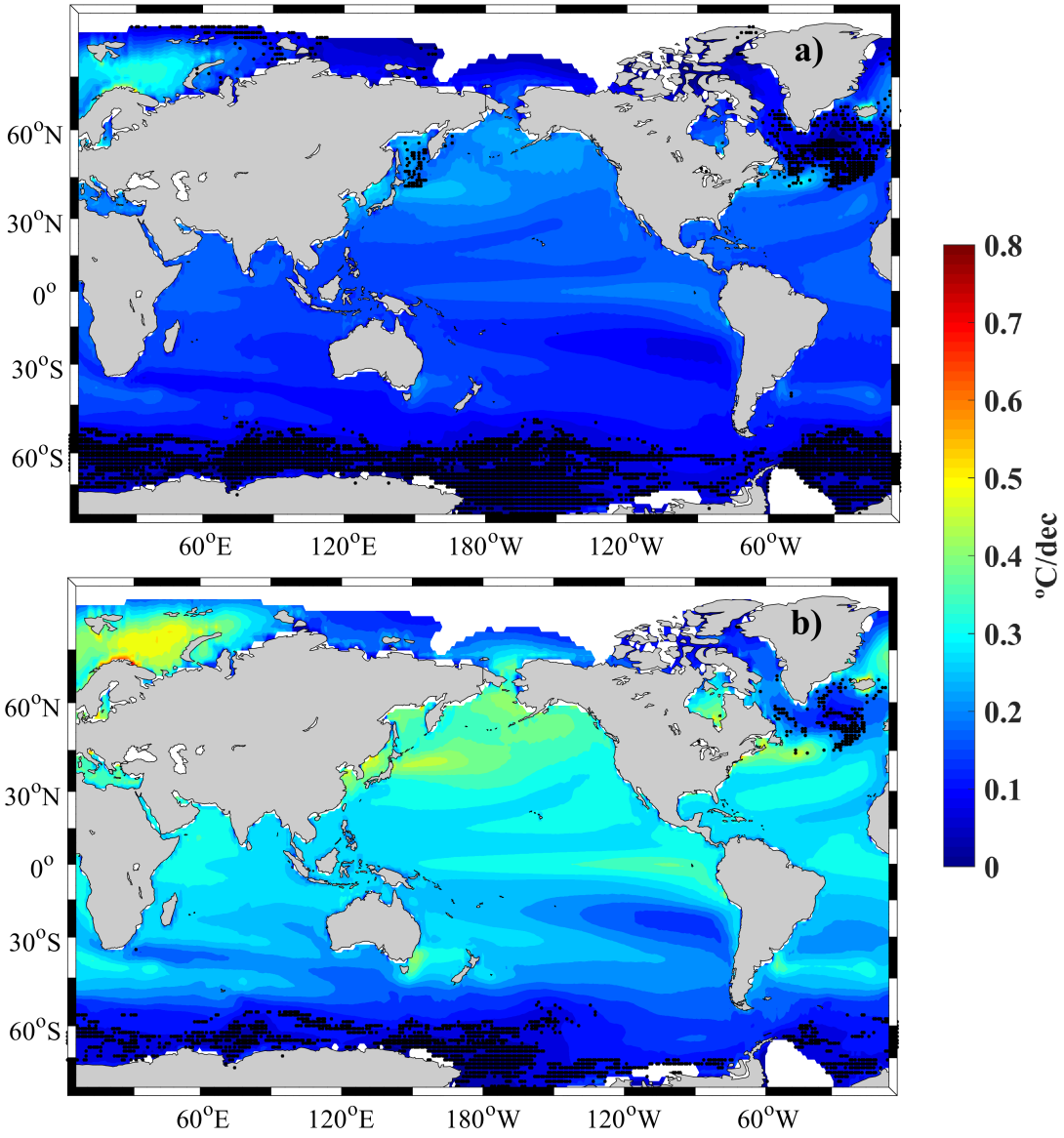

Figure 13: SST trend maps for RCP4.5 (a) and RCP8.5 (b) scenarios between 1975 and 2100. Black dots represent coordinates where consistency is minor than 95% and white areas correspond to the sea ice.

In general, SST trends present an intensification on RCP 8.5 scenario comparing to RCP 4.5 scenario, mainly between 30°N and 30°S, presenting an average trend of approximately 0.3 °C/dec in this area. However, this increase is similar to the increment of 0.35 °C/dec obtained by DeCastro *et al.* (2016)for Somali coastal upwelling (equatorial region), during summer monsoon between 2006 and 2099. On Canary upwelling system (tropical region), Sousa *et al.* (2017a) obtained SST trends (May - August) of 0.20 °C/dec between 2006 and 2009.

This increase may have implications in zonal and meridional circulations, which in turn affect the precipitation and air temperature patterns across the globe. The SST warming is an indicator of global warming, and consequently of the increasing of greenhouses emissions and concentrations, like carbon dioxide. Thus, levels of dissolved carbon will continue to increase and will change the chemistry of seawater, turning it more acid. As referred early, with oceans acidity increase, certain organisms, such as coral and shellfish, will have difficulties to build their skeletons and shells. These effects could substantially affect the biodiversity and productivity of ocean ecosystems.

4 Conclusions

This dissertation was conducted aiming to provide new insights into climate change impacts in future SST variability on a large scale. To achieve this, a set of objectives were defined, being the main conclusions presented in this section.

To assess future SST variability were used results provide by different GCMs of CMIP5. An assessment of the performance of GCMs of CMIP5 on predicting SST was performed by comparative analysis with Era Interim SST data, in order to validate the use of these models forecasts to accomplish the main aim of this study. According to the statistical analysis of Kernel Distribution Estimator and Taylor Diagrams, it was possible to conclude that most of GCMs present good SST predictions. However, some GCMs present poor model performance. In this sense, CSIRO-Mk3-6-0, IPSL-CM5B-LR, MPI-ESM-MR, MPI-ESM-LR, and MRI-CGCM3 were excluded. Thus, a multimodel mean of selected models was found to be best option for this study purposes.

Taking account the multimodel mean, North regions present a higher thermal amplitude comparing with equivalent regions of South areas. In North Hemisphere, SST ranges from -1.5 °C to 32 °C, while in South Hemisphere SST ranges from 0 °C to 32 °C. The winter and summer months are clearly identified for each hemisphere. Thus, it can be concluded that multimodel mean of selected models produce a good prediction and distribution of worldwide SST.

The assessment of SST changes under global warming effects was carried out, allowing to conclude that SST increment reveals a future general warming throughout all the world regions. The monthly mean differences between historical and future periods for both RCP scenarios will be more evident in STRN (3.19 °C, between long-term future (2070 - 2100) and historical period (1975 - 2005)) and TRN (3.09 °C, between long-term future (2070 - 2100) and historical period (1975 - 2005)) regions. Also, higher SST changes will be found on Polar Regions, where warming will have higher impacts.

Taking into account RCP 4.5 and RCP 8.5 scenarios, the North Hemisphere will present higher SST trends, on PRN (1.96 °C and 3.86 °C), STRN (2.64 °C and 4.34 °C) , TRN (2.30 °C and 3.95 °C) and ERN (2.18 °C and 3.84 °C) regions, in agreement with worldwide trends.

Overall, this work analysis predicts that SST will increase worldwide. However, SST increase variability depends on the different globe locations. Thus, this study may be used as a starting point to downscaling studies, that way string new insights on regional scales.

Finally, for future work will be important to replay this study using the same predictive

models, but applying the method of ensemble pattern regression to assess the differences between two multimodel mean methods and evaluate the accurancy of results for future SST changes. To better understand the SST variability will be important to study teleconnectivity and Empirical Orthogonal Functions patterns in order to identify the worldwide spatial and temporal SST patterns. Hereafter, it will be also interesting to study downscaling systems, such as currents and upwelling systems, which have a direct impact on SST changes.

5 Appendix A

Table A. 1: KS-test results for each GCM and region.

GCM	Null-hypothesis								P-value								D-value							
	PRN	STRN	PRN	ERN	ERS	TRS	STRS	PRS	PRN	STRN	PRN	ERN	ERS	TRS	STRS	PRS	PRN	STRN	PRN	ERN	ERS	TRS	STRS	PRS
ACCESS 1-0	0	0	0	0	0	0	0	0	0.98	0.58	0.96	0.99	0.99	0.94	0.99	0.71	0.13	0.19	0.12	0.10	0.11	0.13	0.12	0.22
ACCESS 1-3	0	0	0	0	0	0	0	0	0.84	0.79	0.62	0.54	0.96	0.76	0.99	0.71	0.17	0.16	0.18	0.20	0.16	0.17	0.12	0.22
CanESM2	0	0	0	0	0	0	0	0	0.36	0.95	0.83	0.20	0.99	0.11	0.99	0.09	0.26	0.13	0.15	0.27	0.11	0.30	0.12	0.39
CCSM4	0	0	0	0	0	0	0	0	0.20	0.95	0.96	0.94	0.74	0.93	0.26	0.43	0.30	0.13	0.12	0.13	0.21	0.13	0.27	0.28
CMCC-CM	0	0	0	0	0	0	0	0	0.20	0.99	0.96	0.76	0.99	0.54	0.89	0.94	0.30	0.09	0.12	0.17	0.11	0.20	0.15	0.17
CMCC-CMS	0	0	0	0	0	0	0	0	0.36	0.99	0.96	0.76	0.96	0.54	0.99	0.71	0.26	0.09	0.12	0.17	0.16	0.20	0.12	0.22
CNRM-CM5	0	0	0	0	0	0	0	0	0.84	0.95	0.83	0.76	0.96	0.94	0.89	0.71	0.17	0.13	0.15	0.17	0.16	0.13	0.15	0.22
CSIRO-Mk3-6-0	0	0	0	0	0	0	0	0	0.20	0.80	0.83	0.94	0.74	0.54	0.89	0.71	0.30	0.16	0.15	0.13	0.21	0.20	0.15	0.22
EC-EARTH	0	0	0	0	0	0	0	0	0.36	0.95	0.96	0.20	0.74	0.94	0.99	0.43	0.26	0.13	0.12	0.27	0.21	0.13	0.12	0.28
GISS-E2-H	0	0	0	0	0	0	0	0	0.36	0.58	0.83	0.76	0.74	0.94	0.67	0.43	0.26	0.19	0.15	0.17	0.21	0.13	0.19	0.28
GISS-E2-H-CC	0	0	0	0	0	0	0	0	0.59	0.80	0.62	0.54	0.74	0.99	0.67	0.22	0.21	0.16	0.18	0.20	0.21	0.10	0.19	0.33
GISS-E2-R	0	0	0	0	0	0	0	0	0.84	0.99	0.96	0.76	0.74	0.94	0.99	0.71	0.17	0.09	0.12	0.17	0.21	0.13	0.12	0.22
HadGEM2-AO	0	0	0	0	0	0	0	0	0.59	1.00	0.99	0.99	0.96	0.76	0.99	0.71	0.22	0.06	0.09	0.10	0.16	0.17	0.12	0.22
HadGEM2-CC	0	0	0	0	0	0	0	0	0.36	0.99	0.96	0.99	0.96	0.54	0.99	0.71	0.26	0.09	0.12	0.10	0.16	0.20	0.12	0.22
HadGEM2-ES	0	0	0	0	0	0	0	0	0.59	0.99	0.42	0.94	0.96	0.54	0.99	0.71	0.22	0.09	0.21	0.13	0.16	0.20	0.12	0.22
INMCM4	0	0	0	0	0	0	0	0	0.84	0.95	0.99	0.54	0.74	0.76	0.89	0.71	0.17	0.13	0.09	0.20	0.21	0.17	0.15	0.22
IPSL-CM5A-LR	0	0	0	0	0	0	0	0	0.59	0.99	0.62	0.94	0.96	0.11	0.89	0.71	0.22	0.09	0.18	0.13	0.16	0.30	0.15	0.22
IPSL-CM5A-MR	0	0	0	0	0	0	0	0	0.59	0.95	0.83	0.94	0.74	0.11	0.89	0.71	0.22	0.13	0.15	0.13	0.21	0.30	0.15	0.22
IPL-CM5B-LR	0	0	0	0	0	0	0	0	0.20	0.95	0.42	0.94	0.96	0.54	0.99	0.09	0.30	0.13	0.21	0.13	0.16	0.20	0.12	0.39
MIROC5	0	0	0	0	0	0	0	0	0.59	0.80	0.83	0.99	0.96	0.99	0.89	0.71	0.22	0.16	0.15	0.10	0.16	0.10	0.15	0.22
MIROC-ESM	0	0	0	0	0	0	0	0	0.98	0.99	0.62	0.34	0.99	0.34	0.99	0.43	0.13	0.09	0.18	0.23	0.11	0.23	0.12	0.28
MIROC-ESM-CHEM	0	0	0	0	0	0	0	0	0.84	0.95	0.62	0.20	0.99	0.34	0.89	0.22	0.17	0.13	0.18	0.27	0.11	0.23	0.15	0.33
MPI-ESM-LR	1	0	0	0	0	0	0	0	0.04	0.95	0.96	0.94	1.00	0.76	0.44	0.94	0.39	0.13	0.12	0.13	0.11	0.17	0.23	0.17
MPI-ESM-MR	1	0	0	0	0	0	0	0	0.04	0.95	0.83	0.94	0.99	0.76	0.44	0.94	0.39	0.13	0.15	0.13	0.11	0.17	0.23	0.17
MRI-CGCM3	0	0	0	0	0	0	0	0	0.84	0.58	0.83	0.76	0.46	0.99	0.89	0.43	0.17	0.19	0.15	0.17	0.26	0.10	0.15	0.28
NorESM1-M	0	0	0	0	0	0	0	0	0.59	0.99	0.83	0.76	0.96	0.99	0.67	0.71	0.22	0.09	0.15	0.17	0.16	0.10	0.19	0.22
NorESM1-ME	0	0	0	0	0	0	0	0	0.59	0.95	0.83	0.76	0.74	0.94	0.89	0.09	0.22	0.13	0.15	0.17	0.21	0.13	0.15	0.39

References

Alonso, J., Blázquez, E., Isaza-Toro, E., & Vidal, J. 2015. Internal structure of the upwelling events at Punta Gallinas (Colombian Caribbean) from modis-sst imagery. *Continental Shelf Research*, **109**, 127–134.

Alvarez, I., Ospina-Alvarez, N., Pazos, Y., DeCastro, M., Bernardez, P., Campos, M. J., Gomez-Gesteira, J. L., Alvarez-Ossorio, M. T., Varela, M., Gomez-Gesteira, M., & Prego, R. 2009. A winter upwelling event in the Northern Galician Rias: Frequency and oceanographic implications. *Estuarine, Coastal and Shelf Science*, **82**(4), 573–582.

Alvarez, I., Gomez-Gesteira, M., DeCastro, M., Gomez-Gesteira, J. L., & Dias, J. M. 2010. Summer upwelling frequency along the western Cantabrian coast from 1967 to 2007. *Journal of Marine Systems*, **79**(1-2), 218–226.

Bao, B., & Ren, G. 2014. Climatological characteristics and long-term change of SST over the marginal seas of China. *Continental Shelf Research*, **77**, 96–106.

Barton, E. D., Field, D. B., & Roy, C. 2013. Canary current upwelling: More or less? *Progress in Oceanography*, **116**, 167–178.

Belkin, I. M. 2009. Rapid warming of large marine ecosystems. *Progress in Oceanography*, **81**(1-4), 207–213.

Bindoff, N. L., Stott, P. A., AchutaRao, K. M., Allen, M. R., Gillett, N., Gutzler, D., Hansingo, K., Hegerl, G., Hu, Y., Jain, S., Mokhov, I. I., Overland, J., Perlwitz, J., Sebbari, R., & Zhang, X. 2014. Detection and attribution of climate change: from global to regional. *Climate Change 2013: The Physical Science Basis. Contribution of Working Group I to the Fifth Assessment Report of the Intergovernmental Panel on Climate Change [Stocker, T.F., D. Qin, G.-K. Plattner, M. Tignor, S.K. Allen, J. Boschung, A. Nauels, Y. Xia,*, 1217–1308.

Bjerknes, J. 1969. Atmospheric teleconnections from the equatorial pacific 1. *Monthly Weather Review*, **97**(3), 163–172.

Boer, G. J., Pietrzak, J. D., & Winterwerp, J. C. 2007. SST observations of upwelling induced by tidal straining in the Rhine ROFI. *Continental Shelf Research*, **29**(1), 263–277.

Bony, S., Lau, K. M., & Sud, Y. C. 1996. Sea surface temperature and large-scale circulation influences on tropical greenhouse effect cloud radiative forcing. *Journal of Climate*, **10**(8), 2055–2077.

Bouali, M., Sato, O. T., & Polito, P. S. 2017. Temporal trends in sea surface temperature gradients in the South Atlantic Ocean. *Remote Sensing of Environment*, **194**, 100–114.

Cadule, P., Friedlingstein, P., Bopp, L., Sitch, S., Jones, C. D., Ciais, P., Piao, S. L., & Peylin, P. 2010. Benchmarking coupled climate-carbon models against long-term atmospheric CO$_2$ measurements. *Global Biogeochemical Cycles*, **24**(2), 1–24.

Cane, M. A., Clement, A. C., Kaplan, A., Kushnir, Y., Pozdnyakov, D., Seager, R., Zebiak, S. E., & Murtugudde, R. 1997. Twentieth-century sea surface temperature trends. *Science*, **275**(5302), 957 – 960.

Carvalho, M. J., Melo-Gonçalves, P., Teixeira, J. C., & Rocha, A. 2016. Regionalization of europe based on a K-Means cluster analysis of the climate change of temperatures and precipitation. *Physics and Chemistry of the Earth*, **94**, 22–28.

Chan, D., & Wu, Q. 2015. Attributing observed SST trends and subcontinental land warming to anthropogenic forcing during 1979-2005. *Journal of Climate*, **28**(8), 3152–3170.

Chang, P., Saravanan, R., Ji, L., & Hegerl, G. C. 2000. The effect of local sea surface temperatures on atmospheric circulation over the tropical atlantic sector. *Journal of Climate*, **13**(13), 2195–2216.

DeCastro, M., Gómez-Gesteira, M., Costoya, X., & Santos, F. 2014. Upwelling influence on the number of extreme hot SST days along the Canary upwelling ecosystem. *Journal of Geophysical Research : Oceans*, **119**(1), 1365–1382.

DeCastro, M., Sousa, M. C., Santos, F., Dias, J. M., & Gómez-Gesteira, M. 2016. How will Somali coastal upwelling evolve under future warming scenarios? *Scientific Reports*, **6**(October 2015), 1–9.

DeGaetano, A. T., & Shulman, M. D. 1990. A climatic classification of plant hardiness in the United States and Canada. *Agricultural and Forest Meteorology*, **51**(3-4), 333–351.

DiNezio, P. N., Clement, A. C., Vecchi, G. A., Soden, B. J., Kirtman, B. P., & Lee, S. K. 2009. Climate response of the equatorial pacific to global warming. *Journal of Climate*, **22**(18), 4873–4892.

Environmental Protection Agency, U.S. 2016. *Climate change indicators in the united states,2016.Fourth edition, 96.*

Folland, C . K., Palmer, T. N., & Parker, D. E. 1986. Sahel rainfall and worldwide sea temperatures, 1901-85. *Nature*, **320**, 602.

Fovell, R. G., & Fovell, M. Y C. 1993. Climate zones of the conterminous United States defined using cluster analysis. *Journal of Climate*, **6**(11), 2103–2135.

Gillett, N. P., Stott, P. A., & Santer, B. D. 2008. Attribution of cyclogenesis region sea surface temperature change to anthropogenic influence. *Geophysical Research Letters*, **35**(9), 1–5.

Gleckler, P. J., Taylor, K. E., & Doutriaux, C. 2008. Performance metrics for climate models. *Journal of Geophysical Research Atmospheres*, **113**(6), 1–20.

Goela, Priscila Costa, Cordeiro, Clara, Danchenko, Sergei, Icely, John, Cristina, Sónia, & Newton, Alice. 2016. Time series analysis of data for sea surface temperature and upwelling components from the southwest coast of Portugal. *Journal of Marine Systems*, **163**, 12–22.

Good, P., Lowe, J. A., & Rowell, D. P. 2008. Understanding uncertainty in future projections for the tropical Atlantic: Relationships with the unforced climate. *Climate Dynamics*, **32**(2-3), 205–218.

Hansen, J., Ruedy, R., Sato, M., & Lo, K. 2010. Global surface temperature change. *Revious of Geophysics*, **48**(4), 4004.

Harrison, D. E., & Carson, M. 2007. Is the world ocean warming? Upper-ocean temperature trends: 1950-2000. *Journal of Physical Oceanography*, **37**(2), 174–187.

Hastenrath, S. 1978. On modes of tropical circulation and climate anomalies. *Journal of the Atmospheric Sciences*, **35**, 2222–2231.

He, J., & Soden, B. J. 2016. The impact of SST biases on projections of anthropogenic climate change: A greater role for atmosphere-only models? *Geophysical Research Letters*, **43**(14), 7745–7750.

Hegerl, G. C., Zwiers, F. W., Braconnot, P., Gillett, N. P., Luo, Y., Orsini, J. A. M., Nicholls, N., Penner, J. E., & Stott, P. A. 2007. Understanding and attributing climate change. In: Climate Change 2007: The Physical Science Basis. Contribution of Working Group I to the Fourth Assessment Report of the Intergovernmental Panel on Climate Change. *Cambridge University Press*, **80**(3-4), 213–238.

Huang, P. 2015. Seasonal changes in tropical SST and the surface energy budget under global warming projected by CMIP5 models. *Journal of Climate*, **28**(16), 6503–6515.

Huang, P., & Ying, J. 2015. A multimodel ensemble pattern regression method to correct the tropical pacific SST change patterns under global warming. *Journal of Climate*, **28**(12), 4706–4723.

IPCC. 2014. Climate change 2013: The physical science basis. *The Fifth Assessment Report*, **5**, 1552.

Khalil, I., Atkinson, P. M., & Challenor, P. 2016. Looking back and looking forwards: Historical and future trends in seasurface temperature (SST) in the Indo-Pacific region from 1982 to 2100. *International Journal of Applied Earth Observation and Geoinformation*, **45**, 14–26.

Kolmogorov, A. N. 1933. Sulla determinazione empirica di uma legge di distribuzione. *G.dell Ist. Ital.degli Attuari*, **4**, 83–91.

Legg, T. P., Mylne, K. R., & Woolcock, C. 2002. Use of medium-range ensembles at the Met Office 1: PREVIN - A system for the production of probabilistic forecast information from the ECMWF EPS. *Meteorological Applications*, **9**(3), 255–271.

Lehmann, E. L. 2006. Nonparametrics: Statistical Methods Based on Ranks. 1 edn. Springer-Verlag New York.

Levitus, S., Antonov, J. I., Boyer, T. P., & Stephens, C. 2000. Warming of the world ocean. *Science*, **287**(5461), 2225 – 2229.

Levitus, S., Antonov, J., & Boyer, T. 2005. Warming of the world ocean, 1955-2003. *Geophysical Research Letters*, **32**(2), 1–4.

Levitus, S., Antonov, J. I., Boyer, T. P., Baranova, O. K., Garcia, H. E., Locarnini, R. A., Mishonov, A. V., Reagan, J. R., Seidov, D., Yarosh, E. S., & Zweng, M. M. 2012. World ocean heat content and thermosteric sea level change (0-2000m), 1955-2010. *Geophysical Research Letters*, **39**(10), 1–5.

Lima, F. P., & Wethey, D. S. 2012. Three decades of high-resolution coastal sea surface temperatures reveal more than warming. *Nature Communications*, **3**, 1–13.

Macqueen, J. 1967. Some methods for classification and analysis of multivariate observations. *Proceedings of the Fifth Berkeley Symposium on Mathematical Statistics and Probability*, **1**(233), 281–297.

Marta-Almeida, M., Teixeira, J. C., Carvalho, M. J., Melo-Gonçalves, P., & Rocha, A. M. 2016. High resolution WRF climatic simulations for the Iberian Peninsula: Model validation. *Physics and Chemistry of the Earth*, **94**, 94–105.

Melillo, J. M., Richmond, T. C., & Yohe, W. G. 2014. Climate change impacts in the united states: The third national climate assessment. *United States Global Change Research Program*, 841.

Mikaloff Fletcher, S. E., Gruber, N., Jacobson, A. R., Doney, S. C., Dutkiewicz, S., Gerber, M., Follows, M., Joos, F., Lindsay, K., Menemenlis, D., Mouchet, A., Müller, S. A., & Sarmiento, J. L. 2006. Inverse estimates of anthropogenic CO_2 uptake, transport, and storage by the ocean. *Global Biogeochemical Cycles*, **20**(2), 1–16.

Molteni, F., Buizza, R., Palmer, T. N., & Petroliagis, T. 1996. Analysis of : The ECMWF ensemble prediction system : Methodology and validation. *Q. J. R. Meteorl. Soc*, **122**, 73–119.

Moss, R. H., Edmonds, J. A., Hibbard, K. A., Manning, M. R., Rose, S. K., Van Vuuren, D. P., Carter, T. R., Emori, S., Kainuma, M., Kram, T., Meehl, G. A., Mitchell, J. F. B., Nakicenovic, N., Riahi, K., Smith, S. J., Stouffer, R. J., Thomson, A. M., Weyant, J. P., & Wilbanks, T. J. 2010. The next generation of scenarios for climate change research and assessment. *Nature*, **463**(7282), 747–756.

Nascimento, S., Franco, P., Sousa, F., Dias, J., & Neves, F. 2011. Automated computational delimitation of SST upwelling areas using fuzzy clustering. *Computers and Geosciences*, **43**, 207–216.

Nishii, K., Miyasaka, T., Nakamura, H., Kosaka, Y., Yokoi, S., Takayabu, Y. N., Endo, H., Ichikawa, H., Inoue, T., Oshima, K., Sato, N., & Tsushima, Y. 2012. Relationship of the reproducibility of multiple variables among global climate models. *Journal of the Meteorological Society of Japan*, **90A**(0), 87–100.

Ostrander, G. K., Armstrong, K. M., Knobbe, E. T., Gerace, D., & Scully, E. P. 2000. Rapid transition in the structure of a coral reef community: the effects of coral bleaching and physical disturbance. *Proceedings of the National Academy of Sciences of the United States of America*, **97**(10), 5297–5302.

Parzen, E. 1962. On estimation of a probability density function and mode. *The Annals of Mathematical Statistics*, **33**(3), 1065–1076.

Pincus, R., Batstone, C. P., Patrick Hofmann, R. J., Taylor, K. E., & Glecker, P. J. 2008. Evaluating the present-day simulation of clouds, precipitation, and radiation in climate models. *Journal of Geophysical Research Atmospheres*, **113**(14), 1–10.

Pratchett, M. S., Wilson, S. K., Berumen, M. L., & McCormick, M. I. 2004. Sublethal effects of coral bleaching on an obligate coral feeding butterflyfish. *Coral Reefs*, **23**(3), 352–356.

Press, W. H., Teukolsky, S. A., Vetterling, W. T., & Flannery, B. P. 1992. Numerical Recipes. *Cambrigde University Press*.

Räisänen, J., & Palmer, T. N. 2001. A probability and decision-model analysis of a multimodel ensemble of climate change simulations. *Journal of Climate*, **14**(15), 3212–3226.

Rajagopalan, B., Lall, U., & Tarboton, D. G. 1997. Evaluation of kernel density estimation methods for daily precipitation resampling. *Stochastic Hydrology and Hydraulics*, **11**(6), 523–547.

Reichler, T., & Kim, J. 2008. How well do coupled models simulate today's climate? *Bulletin of the American Meteorological Society*, **89**(3), 303–311.

Rodríguez, R. V. 2017. Worldwide evolution of upwelling and its influence on SST trends. *Phd. Universidad de Vigo*, 162.

Rodwell, M. J., Rowell, D. P., & Folland, C. K. 1999. Oceanic forcing of the wintertime North Atlantic Oscillation and European climate. *Nature*, **398**(6725), 320–323.

Rosenblatt, M. 1956. Remarks on some nonparametric estimates of a density function. *The Annals of Mathematical Statistics*, **27**(3), 832–837.

Rykaczewski, R. R., Dunne, J. P., Sydeman, W. J., García-Reyes, M., Black, B. A., & Bograd, S. J. 2015. Poleward displacement of coastal upwelling-favorable winds in the ocean's eastern boundary currents through the 21st century. *Geophysical Research Letters*, **42**(15), 6424–6431.

Sahany, S., Neelin, J. D., Hales, K., & Neale, R. B. 2014. Deep convective transition characteristics in the community climate system model and changes under global warming. *Journal of Climate*, **27**(24), 9214–9232.

Santos, F., DeCastro, M., Gómez-Gesteira, M., & Álvarez, I. 2012. Differences in coastal and oceanic SST warming rates along the Canary upwelling ecosystem from 1982 to 2010. *Continental Shelf Research*, **47**, 1–6.

Smirnov, N. 1948. Table for Estimating the Goodness of Fit of Empirical Distributions. *The Annals of Mathematical Statistics*, **19**(2), 279–281.

Sousa, M. C., Alvarez, I., DeCastro, M., Gomez-Gesteira, M., & Dias, J. M. 2017a. Seasonality of coastal upwelling trends under future warming scenarios along the southern limit of the canary upwelling system. *Progress in Oceanography*, **153**, 16–23.

Sousa, M. C., DeCastro, M., Alvarez, I., Gomez-Gesteira, M., & Dias, J. M. 2017b. Why coastal upwelling is expected to increase along the western Iberian Peninsula over the next century? *Science of the Total Environment*, **592**, 243–251.

Taylor, K. E. 2001. Summarizing multiple aspects of model performance in a single diagram. *Journal of Geophysical Research: Atmospheres*, **106**(D7), 7183–7192.

Taylor, K. E., Stouffer, R. J., & Meehl, G. A. 2012. An overview of CMIP5 and the experiment design. *Bulletin of the American Meteorological Society*, **93**(4), 485–498.

Tebaldi, C., Arblaster, J. M., & Knutti, R. 2011. Mapping model agreement on future climate projections. *Geophysical Research Letters*, **38**(23), 1–5.

Timmermann, A., Okumura, Y., An, S. I., Clement, A., Dong, B., Guilyardi, E., Hu, A., Jungclaus, J. H., Renold, M., Stocker, T. F., Stouffer, R. J., Sutton, R., Xie, S. P., & Yin, J. 2007. The influence of a weakening of the Atlantic meridional overturning circulation on ENSO. *Journal of Climate*, **20**(19), 4899–4919.

Ting, M., Kushnir, Y., & Li, C. 2013. North Atlantic Multidecadal SST Oscillation: External forcing versus internal variability. *Journal of Marine Systems*, **133**, 27–38.

Van Oldenborgh, G. J., Doblas Reyes, F. J., Drijfhout, S. S., & Hawkins, E. 2013. Reliability of regional climate model trends. *Environmental Research Letters*, **8**(1).

Wang, C., Zhang, L., Lee, S. K., Wu, L., & Mechoso, C. R. 2014. A global perspective on CMIP5 climate model biases. *Nature Climate Change*, **4**(3), 201–205.

Wang, D., Gouhier, T. C., Menge, B. A., & Ganguly, A. R. 2015. Intensification and spatial homogenization of coastal upwelling under climate change. *Nature*, **518**(7539), 390–394.

Wang, M., Overland, J. E., & Bond, N. A. 2010. Climate projections for selected large marine ecosystems. *Journal of Marine Systems*, **79**(3-4), 258–266.

Waugh, D. W., & Eyring, V. 2008. Quantitative performance metrics for stratospheric-resolving chemistry-climate models. *Atmospheric Chemistry and Physics Discussion*, 5699–5713.

Whitney, H.B., & Mann, D. R. 1947. On a test of whether one of two random variables is stochastically larger than the other. *The Annals of Mathematical Statistics*, **18**(1), 50–60.

Wilks, D. S. 2006. Statistical Methods in the Atmospheric Sciences. *Meteorological Applications*, **14**, 627.

Xie, S. P., Deser, C., Vecchi, G. A., Ma, J., Teng, H., & Wittenberg, A. T. 2010. Global warming pattern formation: Sea surface temperature and rainfall. *Journal of Climate*, **23**(4), 966–986.

Xu, H., Kim, H. M., Nye, J. A., & Hameed, S. 2015. Impacts of the North Atlantic Oscillation on sea surface temperature on the Northeast US Continental Shelf. *Continental Shelf Research*, **105**, 60–66.

Yin, J., Schlesinger, M. E., & Stouffer, R. J. 2009. Model projections of rapid sea-level rise on the northeast coast of the United States. *Nature Geoscience*, **2**, 262.

Yin, J., Griffies, S. M., & Stouffer, R. J. 2010. Spatial variability of sea level rise in twenty-first century projections. *Journal of Climate*, **23**(17), 4585–4607.

Yokoi, S., Takayabu, Y. N., Nishii, K., Nakamura, H., Endo, H., Ichikawa, H., Inoue, T., Kimoto, M., Kosaka, Y., Miyasaka, T., Oshima, K., Sato, N., Tsushima, Y., & Watanabe, M. 2011. Application of cluster analysis to climate model performance metrics. *Journal of Applied Meteorology and Climatology*, **50**(8), 1666–1675.

Yoon, J., Yeh, S. W., Kim, Y. H., Kug, J. S., & Min, H. S. 2012. Understanding the responses of sea surface temperature to the two different types of El Niño in the western North Pacific. *Progress in Oceanography*, **105**, 81–89.